

Pyridine-Derived N-Heterocyclic Carbenes: An Experimental and Theoretical Evaluation of the Bonding in and Reactivity of Selected Normal and Abnormal Complexes of Nickel(II) and Palladium(II)

Elzert Stander-Grobler,[†] Oliver Schuster,^{*,†,⊥} Greta Heydenrych,[‡] Stephanie Cronje,[†] Evangeline Tosh,[§] Martin Albrecht,[⊥] Gernot Frenking,^{*,‡} and Helgard G. Raubenheimer^{*,†}

[†]Department of Chemistry and Polymer Science, University of Stellenbosch, Private Bag X1, Matieland, 7602, Stellenbosch, South Africa, [‡]Fachbereich Chemie, Philipps-Universität Marburg, Hans-Meerwein-Strasse, D-35043 Marburg, Germany, [§]Inorganic Chemistry Department, Technische Universität München, Lichtenbergstrasse 4, D-85747 Garching, Germany, and [⊥]Department of Chemistry, University of Fribourg, Chemin du Musée 9, CH-1700 Fribourg, Switzerland

Received May 6, 2010

We report a thorough investigation of a series of isomeric complexes with the general formula *trans*-(pyridylidene)M(PPh₃)₂Cl (M = Pd, Ni). For the first time, a systematic comparison of *normal*, *abnormal*, and *remote* bonding modes is presented. X-ray structural and ¹³C NMR data indicate the importance of carbenoid mesomeric contributions in their compound class. The catalytic performance of the palladium complexes *trans*-(pyridylidene)Pd(PPh₃)₂Cl as precursors in Suzuki–Miyaura-type cross-coupling suggests a correlation of *remote* bonding with catalyst robustness and effectivity. When metal precursors M(PPh₃)₄ are reacted with 2,4-dichloropyridinium salts, preferential formation of *remote* carbene complexes occurs and indications are that electronic parameters rather than steric influences are responsible for the observed selectivity. Calculations at the BP86/TZ2P level of theory support interpretation of the results.

Introduction

The chemistry of N-heterocyclic carbenes (NHCs) has seen an explosive development during the last number of years.^{1–5} However, despite the vast number of possible N-heterocycles that could be classified as carbenes, the activity in NHC chemistry has concentrated by and large on 2-imidazolylidenes, often called “Arduengo” carbenes.^{1–5} Only recently has it been shown that an abnormal binding mode via the C4 (or C5) position of imidazolylidenes yields

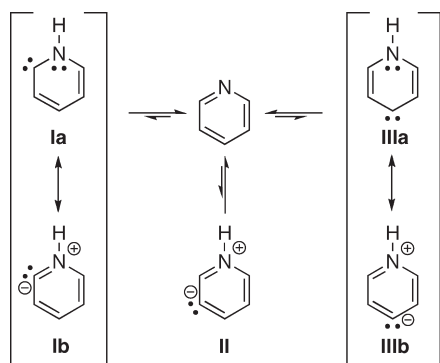
extraordinary electron-rich metal centers.^{6–17} These discoveries led to a considerably increased interest in “nonclassical” NHCs, i.e., carbenes that are not stabilized by two adjacent heteroatoms.¹⁸ We have been active in this field for a decade and have investigated in particular pyridinium-derived carbenes.^{19–25} With now well-established protocols for the functionalization of pyridine, pyridylidenes offer great potential for variation of steric demand and electronic properties. Moreover, they can bind to the metal in a *normal* (**I**, **III**) or *abnormal* (**II**) fashion (Scheme 1) with the possibility of

*To whom correspondence should be addressed. E-mail: oliver.schuster@unifr.ch.

- Bertrand G., Ed. *J. Organomet. Chem.* **2005**, 690 (24–25).
- Crabtree R. H., Ed. *Coord. Chem. Rev.* **2007**, 251 (5–6).
- Glorius F. Ed. *Top. Organomet. Chem.* **2007**, 21.
- Nolan, S. P. *N-Heterocyclic Carbenes in Synthesis*; Wiley-VCH: Weinheim, 2006.
- Hahn, F. E.; Jahnke, M. C. *Angew. Chem., Int. Ed.* **2008**, 47, 3122.
- Gruendemann, S.; Kovacevic, A.; Albrecht, M.; Faller, J. W.; Crabtree, R. H. *Chem. Commun.* **2001**, 2274.
- Gruendemann, S.; Kovacevic, A.; Albrecht, M.; Faller, J. W.; Crabtree, R. H. *J. Am. Chem. Soc.* **2002**, 124, 10473.
- Kluser, E.; Neels, A.; Albrecht, M. *Chem. Commun.* **2006**, 4495.
- Heckenroth, M.; Kluser, E.; Neels, A.; Albrecht, M. *Angew. Chem., Int. Ed.* **2007**, 46, 6293.
- Tonner, R.; Heydenrych, G.; Frenking, G. *Chem.–Asian J.* **2007**, 2, 1555.
- Tonner, R.; Heydenrych, G.; Frenking, G. *ChemPhysChem* **2008**, 9, 1474.
- Yang, L.; Kruger, A.; Neels, A.; Albrecht, M. *Organometallics* **2008**, 27, 3161.
- Albrecht, M. *Chem. Commun.* **2008**, 3601.

- Heckenroth, M.; Albrecht, M. *Chimia* **2008**, 62, 253.
- Heckenroth, M.; Kluser, E.; Neels, A.; Albrecht, M. *Dalton Trans.* **2008**, 6242.
- Heckenroth, M.; Neels, A.; Garnier, M. G.; Aebi, P.; Ehlers, A. W.; Albrecht, M. *Chem.–Eur. J.* **2009**, 15, 9375.
- Aldeco-Perez, E.; Rosenthal, A. J.; Donnadiu, B.; Parameswaran, P.; Frenking, G.; Bertrand, G. *Science* **2009**, 326, 556.
- Schuster, O.; Yang, L.; Raubenheimer, H. G.; Albrecht, M. *Chem. Rev.* **2009**, 109, 3445.
- Raubenheimer, H. G.; Toerien, J. G.; Kruger, G. J.; Otte, R.; van Zyl, W.; Olivier, P. *J. Organomet. Chem.* **1994**, 466, 291.
- Schneider, S. K.; Roembke, P.; Julius, G. R.; Raubenheimer, H. G.; Herrmann, W. A. *Adv. Synth. Catal.* **2006**, 348, 1862.
- Schneider, S. K.; Julius, G. R.; Loschen, C.; Raubenheimer, H. G.; Frenking, G.; Herrmann, W. A. *Dalton Trans.* **2006**, 1226.
- Schneider, S. K.; Rentsch, C. F.; Krueger, A.; Raubenheimer, H. G.; Herrmann, W. A. *J. Mol. Catal. A: Chem.* **2007**, 265, 50.
- Raubenheimer, H. G.; Cronje, S. *Dalton Trans.* **2008**, 1265.
- Heydenrych, G.; von Hopffgarten, M.; Stander, E.; Schuster, O.; Raubenheimer, H. G.; Frenking, G. *Eur. J. Inorg. Chem.* **2009**, 1892.
- Strasser, C. E.; Stander-Grobler, E.; Schuster, O.; Cronje, S.; Raubenheimer, H. G. *Eur. J. Inorg. Chem.* **2009**, 1905.

Scheme 1. Isomeric Pyridine and Pyridylidenes



both *normal* and *abnormal* carbenes arising in a *remote* position (**II**, **III**). We have extended Crabtree's terminology^{6,7} by using the term *abnormal* whenever it is not possible to illustrate the carbene structure without charge separation (in contrast to **Ia** and **IIIa**).¹⁸ *Remote* denotes a carbene that contains no stabilizing heteroatom directly adjacent to the carbene carbon. Accordingly, isomer **II** is *abnormal* and *remote*, whereas isomer **III** is *normal* and *remote*.

Previous theoretical investigations of the *free* ligands indicate that pyridine is by far more stable (0.0 kcal/mol) than the most stable carbenoid isomer **I** (ca. 40 kcal mol⁻¹), while the *remote* species **II** and **III** are even higher in energy (both ca. 55 kcal mol⁻¹).^{24,26,27} Interestingly, calculations of isodesmic reactions by Kassae et al. suggest a similar stabilization of the methylene fragment in 2- and 4-pyridylidenes.²⁸ Significant barriers for *intramolecular* interconversion allowed for detecting the coexistence of isomers **I** and **II** under high-vacuum conditions.^{26,27} In the condensed phase, *intermolecular* interconversion is more facile, and pyridylidenes have thus far been observed only in complexes, i.e., stabilized by a metal center.²⁹ Such metal-stabilized pyridylidenes have been accessible in a few cases by a ligand isomerization process involving a formal proton shift from carbon to nitrogen. Depending on the ring substitution pattern, both 2- and 4-pyridylidene complexes have been prepared by such a rearrangement from *N*-protonated pyridinium salts.^{30–34} In contrast, C–H activation of *N*-alkylated pyridinium precursors that could allow for C2- or

C4-coordination exclusively leads to metalation at the 4-position.^{35–39} This observation has been attributed to the steric bulk of the *N*-alkyl group.

We first carried out a thorough investigation of a series of isomeric complexes with the general formula *trans*-(pyridylidene)M(PPh₃)₂Cl (M = Pd, Ni) using various experimental and computational parameters. We were particularly interested in evaluating whether certain mesomeric contributions would be particularly significant and if the concept of *abnormal* carbene bonding, which is defined on the basis of simple valence bond considerations, transfers to experimental observations. Second, the catalytic performance of the palladium complexes *trans*-(pyridylidene)Pd(PPh₃)₂Cl as precursors in Suzuki–Miyaura-type cross-coupling reactions was studied in order to elucidate the influence of *normal*, *abnormal*, or *remote* carbene bonding. Finally, we investigated preferential carbene complex formation by oxidative addition using low-valent metal precursors and 2,4-dichloropyridinium salts. DFT calculations were used to support our interpretation of the results. As an extension of our studies on quinolyldiene complexes,^{20,21,23,40–42} we also determined the reactivity of M(PPh₃)₄ (M = Pd, Ni) toward 4,7-dichloroquinolinium salts, wherein both chloro substituents are located three bonds away from the nitrogen atom.

Throughout this article, carbene complexes are drawn with M=C double bonds where applicable. Our choice of representation should not be regarded as a statement concerning the actual bond order; it merely helps the reader to identify formal (*normal*) carbene metal bonds.

Results and Discussion

a. Synthesis of 2-, 3-, and 4-Pyridylidene Metal Complexes.

The synthetic routes used to prepare two complete series of ionic 2-, 3-, and 4-pyridylidene metal complexes **3** and **4** are summarized in Scheme 2 and follow our established strategy that has been reported earlier.²³ Pyridinium triflates (triflate = OTf = trifluoromethanesulfonate) were prepared from the corresponding chloropyridines **1a–c** with one equivalent of methyltriflate in dry dichloromethane. Subsequent oxidative addition of the ligand precursor salts to Ni(PPh₃)₄ in THF at room temperature afforded the desired yellow cationic complexes **4** in good yields. Similar procedures in toluene at 60 °C were followed to obtain the corresponding colorless palladium complexes **3**. The oxidative addition leading to the *abnormal* complex **3b** occurred significantly slower than the corresponding reaction for *normal* carbenes.

b. Single-Crystal Structure Determinations. The ORTEP drawing of the molecular structure of the nickel complex **4b** in Figure 1 is representative for the square-planar geometry generally observed for complexes **3** and **4**, as previously established for BF₄ analogues of the 2- and 4-pyridylidene metal complexes.^{20,21} The phosphine ligands adopt the usual *trans* configuration. Unlike the corresponding complexes **3a** and **4a** or **3c** and **4c** (in the BF₄ salt), which crystallize in distinct packing arrangements,^{20,21} crystals of **3b** and **4b** (in the OTf salt) are isomorphous. Relevant parameters for the entire

(26) Lavorato, D. J.; Terlouw, J. K.; Dargel, T. K.; Koch, W.; McGibbon, G. A.; Schwarz, H. *J. Am. Chem. Soc.* **1996**, *118*, 11898.

(27) Lavorato, D. J.; Terlouw, J. K.; McGibbon, G. A.; Dargel, T. K.; Koch, W.; Schwarz, H. *Int. J. Mass Spectrom.* **1998**, *180*, 7.

(28) Kassae, M. Z.; Shakib, F. A.; Momeni, M. R.; Ghambarian, M.; Musavi, S. M. *Tetrahedron* **2009**, *65*, 10093.

(29) Holloczki, O.; Nyulaszi, L. *J. Org. Chem.* **2008**, *73*, 4794.

(30) Weisman, A.; Gozin, M.; Kraatz, H. B.; Milstein, D. *Inorg. Chem.* **1996**, *35*, 1792.

(31) Cave, G. W. V.; Hallett, A. J.; Errington, W.; Rourke, J. P. *Angew. Chem., Int. Ed.* **1998**, *37*, 3270.

(32) Newman, C. P.; Clarkson, G. J.; Alcock, N. W.; Rourke, J. P. *Dalton Trans.* **2006**, 3321.

(33) Alvarez, E.; Conejero, S.; Paneque, M.; Petronilho, A.; Poveda, M. L.; Serrano, O.; Carmona, E. *J. Am. Chem. Soc.* **2006**, *128*, 13060.

(34) Alvarez, E.; Conejero, S.; Lara, P.; Lopez, J. A.; Paneque, M.; Petronilho, A.; Poveda, M. L.; del Rio, D.; Serrano, O.; Carmona, E. *J. Am. Chem. Soc.* **2007**, *129*, 14130.

(35) Cordone, R.; Harman, W. D.; Taube, H. *J. Am. Chem. Soc.* **1989**, *111*, 2896.

(36) Koizumi, T.; Tomon, T.; Tanaka, K. *Organometallics* **2003**, *22*, 970.

(37) Koizumi, T.; Tomon, T.; Tanaka, K. *J. Organomet. Chem.* **2005**, *690*, 1258.

(38) Albrecht, M.; Stoeckli-Evans, H. *Chem. Commun.* **2005**, 4705.

(39) Koizumi, T.; Tomon, T.; Tanaka, K. *J. Organomet. Chem.* **2005**, *690*, 4272.

(40) Meyer, W. H.; Deetlefs, M.; Pohlmann, M.; Scholz, R.; Esterhuysen, M. W.; Julius, G. R.; Raubenheimer, H. G. *Dalton Trans.* **2004**, 413.

(41) Schneider, S. K.; Roembke, P.; Julius, G. R.; Loschen, C.; Raubenheimer, H. G.; Frenking, G.; Herrmann, W. A. *Eur. J. Inorg. Chem.* **2005**, 2973.

(42) Schuster, O.; Raubenheimer, H. G. *Inorg. Chem.* **2006**, 7997.

Scheme 2. Preparation of Two Complete Series of Carbene Complexes

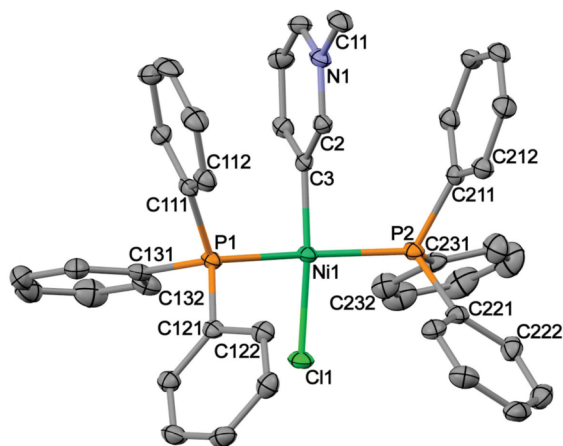
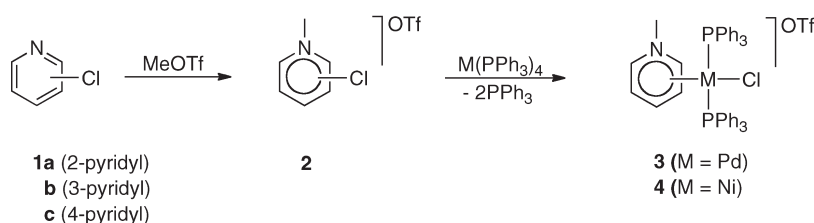


Figure 1. Molecular structure of the cationic complex **4b** (50% probability ellipsoids, hydrogen atoms and counterion omitted).

series of isomeric cationic structures are summarized in Table 1.

As stated earlier,¹⁸ examination of M–C distances is not a versatile tool to prove or rule out carbene-type bonding because differences are usually not significant. Similarly, hindered rotation about the M–C bond does not seem to reflect increased M–C bond order.⁴³

On the other hand, the observed static *trans* influences seem to show a consistent trend: the further the heteroatom occurs from the carbene carbon atom, the longer the *trans* M–Cl bond becomes. Bond lengthening is accompanied by a decrease in the internal bond angle at the carbene carbon (CCX; X = N, C). However, the differences are small and might be influenced by intermolecular dipole–dipole interactions in the solid state.⁴⁴

(43) As a possible indicator for a hindered rotation around the metal carbon bond and hence an increased metal–carbon bond order, we investigated the angles between the mean square planes of the pyridylidene ring and the coordination spheres. Given the fact that an in-plane arrangement is prevented by the bulky phosphine ligands, efficient π back-bonding should result in an orthogonal alignment. Notably, both 4-pyridylidene ligands in the two complexes **3c** and **4c** deviate considerably from this ideal geometry. We are however hesitant to ascribe this observation to an electronic effect because steric considerations seem to prevail (cf. Supporting Information).

(44) Jonas, V.; Frenking, G.; Reetz, M. T. *J. Am. Chem. Soc.* **1994**, *116*, 8741.

(45) Owen, J. S.; Labinger, J. A.; Bercaw, J. E. *J. Am. Chem. Soc.* **2004**, *126*, 8247.

(46) We mention that reinvestigation of the crystal structure of **3a** (in the tetrafluoroborate salt) revealed disorder of the pyridylidene ligand (sof: 0.2), which was not found when the result was published initially.²⁰ The updated structure and selected data can be found in the Supporting Information. However, the disorder compromises a closer examination of the bond distances and angles in the carbene ligand, and we shall therefore concentrate on the nickel complexes, which also, in general, offered better data.

Bercaw and co-workers have discussed the bonding situation for *normal* pyridylidene complexes in terms of the bond alternation within the heterocyclic carbene ligand.⁴⁵ We followed a similar approach in our efforts to identify relevant contributing structures for complexes **4** (Scheme 3).⁴⁶

The 2-pyridylidene moiety in **4a** shows a significant increase in the N1–C6 and C2–C3 distances when compared to free pyridine (Figure 2). However, the N1–C2 bond remains short. These observations could indicate the relative importance of contributing structures such as **IVa** and **IVe** in Scheme 3. A weak diene-type character of 2-pyridylidenes has been suggested earlier.⁴⁷ Remarkably, examination of available structural data on 2-pyridone reveals a rather similar bond distribution pattern therein (Figure 2).

Evidence for a diene-like contribution such as **VIe** (Scheme 3) is also found in the 4-pyridylidene ligand of **4c**. The lateral bonds C2–C3 and C5–C6 are significantly (4.3σ) shorter than those of C3–C4 and C4–C5 (Figure 2). Related bond variations are also found for 4-pyridylidene tungsten²⁵ and platinum complexes.³¹ The latter comprise a short Pt–C bond and a ¹³C carbene resonance as high as 324 ppm. Again, a similar geometry is featured by the corresponding 4-pyridone (Figure 2).

In contrast to the heterocyclic rings of the two *normal* pyridylidene ligands in **4a** and **4c**, where internal distances qualitatively support carbenoid mesomers (**IVe** and **VIe**, respectively), the *abnormal* bonding in complex **4b** entails bond length variations that cannot be readily described in terms of simple valence bond resonance theory. Nevertheless, consistent with the examples above, bonds that involve the nitrogen atom are relatively short (N1–C2, N1–C6), while bonds from the carbene carbon atom are rather long (C2–C3, C3–C4).

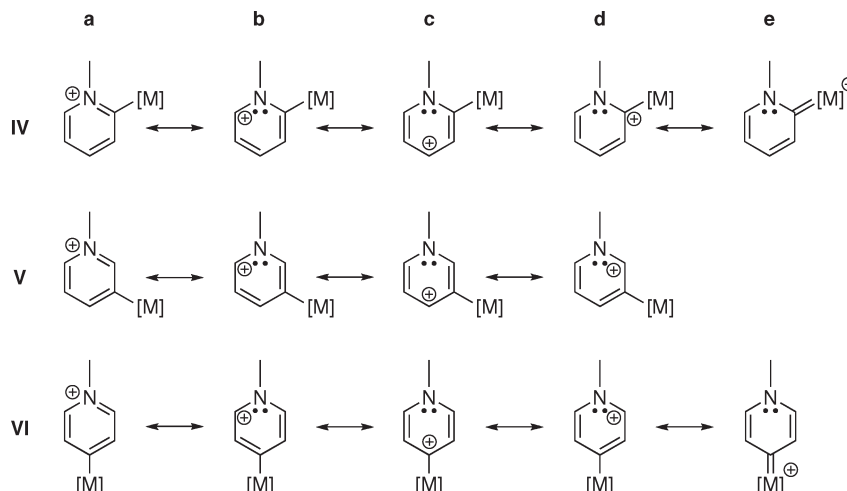
Such findings are particularly relevant when considering that the bond length variations found in complexes **4** are not observed in the corresponding chloropyridinium precursor salts (see Supporting Information for details). In contrast to the situation in the metal complexes, the atom separations are not significantly dependent on the substitution pattern and are closely related to those in unsubstituted pyridinium salts. We therefore conclude that metalation, rather than alkylation, has the greatest influence on the bonding within the heterocyclic ligands during ylidene formation from chloropyridines. Furthermore, this influence of the metal fragment seems to be related to the effect that a doubly bound oxygen exerts in pyridones. These arguments all point toward a non-negligible double-bond character of the metal carbon bonds in the *normal* pyridylidene complexes.

(47) Conejero, S.; Lara, P.; Paneque, M.; Petronilho, A.; Poveda, M. L.; Serrano, O.; Vattier, F.; Alvarez, E.; Maya, C.; Salazar, V.; Carmona, E. *Angew. Chem., Int. Ed.* **2008**, *47*, 4380.

Table 1. Selected Structural Parameters of the Series of Pyridylidene Complexes

	$d(\text{M}-\text{C})$ [Å]	$d(\text{M}-\text{Cl})$ [Å]	CCX angle [deg]	torsion ^a [deg]	distortion ^b [Å]
3a	2.002(3) ^c	2.3638(8)	116.22 ^c	88.60 ^c	0.628 ^c
3b	1.996(7)	2.371(2)	117.82	88.21	0.572
3c^d	1.979(7)	2.3938(17)	114.64	77.84	0.155
4a^e	1.861(5)	2.203(1)	116.84	90.00	1.161
4b	1.874(3)	2.2055(8)	116.23	88.81	0.698
4c^e	1.863(5)	2.2172(13)	115.04	83.46	0.228

^a Angle between the mean square planes defined by (i) the six atoms of the heterocycle (plane1) and (ii) the metal center and the four atoms bound to the metal (plane2). ^b Distance of the metal-bound carbon atom from plane2 as a probe for the distortion of the square-planar geometry. ^c Inaccurate, due to disorder of the ligand (cf. Supporting Information). ^d Ref 20. ^e Ref 21.

Scheme 3. Various Mesomeric Structures of Normal (IV, VI) and Abnormal (V) Pyridylidene Complexes, Some of Them Remote (V, VI)

Interestingly, the *nonmethylated* 4-pyridyl ligand in palladium complex **A** (Figure 3) displays similar features to those of the pyridylidene ligand in **4c**, i.e., short lateral bonds.⁴⁹ It could be reasoned that coordination to the metal center already induces localization of double bonds in a carbenoid fashion (**A'**). Indeed, according to electron decomposition analysis (EDA), σ and π orbital contributions in pyridyl–metal and pyridylidene–metal bonds are remarkably similar.²⁴ This result also provides an explanation for the increased basicity of the nitrogen in pyridyl metal complexes, which can even lead to the activation of dichloromethane.^{50–55}

c. NMR Spectroscopic Characterization. Similar to the difficulties experienced when attempting to determine “carbene character” from metal–carbene bond lengths, a comparison of absolute carbene carbon NMR shift values also does not give clear answers.¹⁸ We have previously noted that correlation of NMR data with data of other analytical techniques, e.g., IR $\nu(\text{CO})$ stretching frequencies, is often poor,

thus requiring cautious interpretation.¹⁸ In the series of complexes **3** and **4**, significantly lower chemical shifts are observed for the *abnormal* complexes **3b** and **4b** (δ_{C} 165 and 174, respectively) than for the *normal* congeners ($\delta_{\text{C}} > 190$). When compared to the corresponding carbon resonances in the precursor pyridinium salts, deshielding between 30 and 50 ppm occurs upon formal carbene formation. For both metals, *abnormal* C3 bonding induces the smallest and *normal* remote C4 bonding the largest shift difference. Nickel bonding shows consistently a stronger deshielding effect than palladium coordination.

In order to correlate the structural investigations with solution properties, we also elucidated the electronic influence of alkylation and metalation on the heterocyclic ring by NMR spectroscopy. Comprehensive interpretation of the ¹H NMR chemical shifts is hampered by the phosphine signals in the aromatic region that overlap with the protons of the heterocycle. Hence, we concentrated on ¹³C NMR data, which are known to be less affected by long-range magnetic and solvent effects⁵⁶ and which correlate well with ¹H data in aromatic systems.^{56,57} Figure 4 summarizes the most relevant chemical shifts.

Linear correlations between the chemical shift and the charge density on a given atom in a homologous series of compounds are often used for the interpretation of NMR results.⁵⁸ Using calculated charge densities, such a dependence has been shown to exist for azine derivatives,⁵⁹ as well

(48) Bruno, I. J.; Cole, J. C.; Edgington, P. R.; Kessler, M.; Macrae, C. F.; McCabe, P.; Pearson, J.; Taylor, R. *Acta Crystallogr., Sect. B: Struct. Sci.* **2002**, *58*, 389.

(49) Meguro, H.; Koizumi, T.; Yamamoto, T.; Kanbara, T. *J. Organomet. Chem.* **2008**, *693*, 1109.

(50) Isobe, K.; Nakamura, Y.; Miwa, T.; Kawaguchi, S. *Bull. Chem. Soc. Jpn.* **1987**, *60*, 149.

(51) Crociani, B.; Di Bianca, F.; Giovenco, A.; Berton, A.; Bertani, R. *J. Organomet. Chem.* **1989**, *361*, 255.

(52) Crociani, B.; Di Bianca, F.; Fontana, A.; Bertani, R. *J. Organomet. Chem.* **1992**, *425*, 155.

(53) Canovese, L.; Uguagliati, P.; Bianca, F. D.; Crociani, B. *J. Organomet. Chem.* **1992**, *438*, 253.

(54) Crociani, B.; Di Bianca, F.; Fontana, A.; Forsellini, E.; Bombieri, G. *J. Chem. Soc., Dalton Trans.* **1994**, 407.

(55) Canovese, L.; Visentin, F.; Uguagliati, P.; Di Bianca, F.; Fontana, A.; Crociani, B. *J. Organomet. Chem.* **1996**, *525*, 43.

(56) Lauterbur, P. C. *Tetrahedron Lett.* **1961**, *2*, 274.

(57) Retcofsky, H. L.; McDonald, F. R. *Tetrahedron Lett.* **1968**, 2575.

(58) Hesse, M.; Meier, H.; Zeeh, B. *Spectroscopic Methods in Organic Chemistry*; Thieme: Stuttgart, 2008.

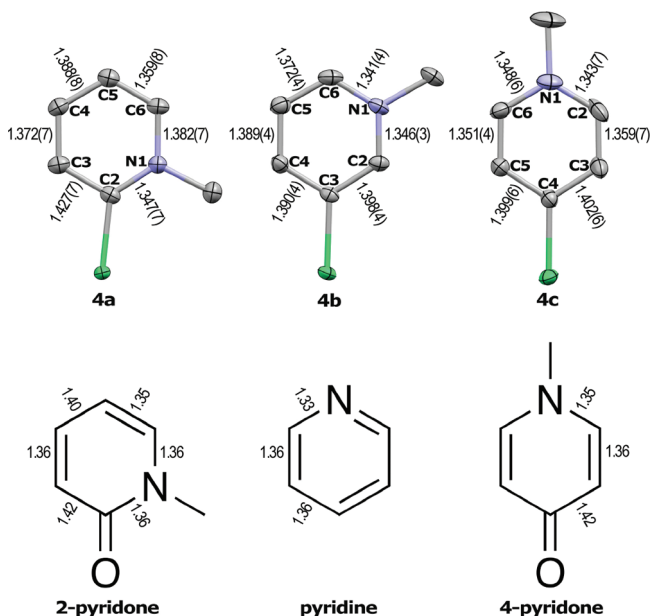


Figure 2. Bond distances (Å) in **4a**, **4b**, and **4c** (top) in comparison to those in free pyridine and pyridones. (Bottom) Data derived from CCSD.⁴⁸

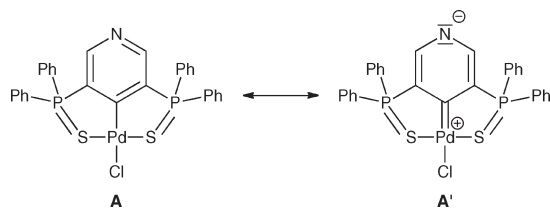


Figure 3. Metal-induced carbenoid electron distribution prior to formal carbene formation (via methylation or protonation).

as for palladium pyridyl complexes.⁶⁰ The latter complexes, however, show a specific behavior for the metal-bound carbons, which can be attributed to anisotropic effects.^{61–63} In our series of compounds, linear regression of the calculated charges in **1a–c**⁶⁴ and experimental NMR measurements (Figure 4) also yields an appreciable fit ($R^2 = 0.91$; see Supporting Information). We therefore assume that the ¹³C NMR data of the heterocyclic carbons that are *not* bound to the metal offer a qualitative probe for the partial charge (re)distributions during complex formation. Information about relative charge densities at the nitrogen atom can be derived indirectly through the N-methyl carbon resonance.⁶⁵ Counterion effects may be insignificant since the triflate salts show negligible alteration of shifts when compared to the corresponding BF₄[−] analogues, some of which have been reported earlier.^{20,21}

(59) Lauterbur, P. C. *J. Chem. Phys.* **1965**, *43*, 360.

(60) Isobe, K.; Kai, E.; Nakamura, Y.; Nishimoto, K.; Miwa, T.; Kawaguchi, S.; Kinoshita, K.; Nakatsu, K. *J. Am. Chem. Soc.* **1980**, *102*, 2475.

(61) Spiesecke, H.; Schneider, W. G. *J. Chem. Phys.* **1961**, *35*, 722.

(62) Kutzelnigg, W. *Isr. J. Chem.* **1980**, *19*, 193.

(63) Kutzelnigg, W.; Fleischer, U.; Schindler, M. *Basic Princ. Prog.* **1990**, *23*, 165.

(64) Feshin, V. P.; Feshina, E. V.; Zhizhina, L. I. *J. Heterocycl. Chem.* **2006**, *42*, 1435.

(65) Wehrli, F. W.; Giger, W.; Simon, W. *Helv. Chim. Acta* **1971**, *54*, 229.

On the basis of these considerations, nitrogen methylation of the chloropyridines **1a–c** affects mostly the region remote to the nitrogen atom. Evidently, the heteroatom — now with increased effective electronegativity — compensates for the loss of its lone pair by draining electron density from the ring and thus decreases the electron density especially at the 4-position significantly in the pyridinium salts **2** regardless of the chloro-substitution pattern. Even though the upfield shift for C2 and C6 is marginal, it might be attributed to a decrease in the N1–C2 and N1–C6 bond orders.⁶⁶

Subsequent metal insertion at the 2-position of **2a** to form **3a** or **4a** induces a drift of the positive charge in the ring toward the vicinity of the metal, thus indicating contributions from resonance structures **IVa**, **IVd**, and **IVe** (cf. Scheme 3). Simultaneously, a secondary process apparently increases the electron density at the carbon atoms that are remote to the coordination site. Owing to this effect, the ¹³C NMR chemical shifts of the neutral starting compound **1** are somewhat restored in the ligand backbone, which is in agreement with predominant charge stabilization within the N–C_{carbene}–M moiety.

The importance of contributing structures similar to **VIc** and **VIe** (Scheme 3) for the *remote* 4-pyridylidene complexes **3c** and **4c** is reflected by a significant charge redistribution within the heterocycle upon carbene formation. Again, metal insertion effects deshielding of the carbon atoms adjacent to the metal-bound carbon and concurrent shielding of the remote nuclei. Even the nitrogen atom possibly becomes less positively charged, as is shown by a small upfield shift for the attached methyl group. Due to the mutual *trans* arrangement of nitrogen and carbene carbon atoms, the polarization in the complex is sufficiently large to render the carbons in *ortho* and *meta* position almost magnetically equivalent. This result lends further support to the carbene character of C4-pyridylidene complexes (**VIe**, cf. X-ray discussion), and it is also in agreement with NBO analysis, which revealed that a Lewis structure resembling **IIIa** (Scheme 1) is most appropriately describing a *free* 4-pyridylidene.⁶⁷

For *abnormal* C3-pyridylidene complexes, interpretation of the NMR results in terms of valence bond theory is not straightforward, thus paralleling the solid-state conclusions. However, the ¹³C NMR data indicate consistently for all pyridylidenes that metalation induces a deshielding effect in the vicinity of the metal combined with shielding of the remote heterocyclic nuclei. Similar observations have also been made by Isobe and co-workers⁵⁰ for neutral non-methylated bromopyridines upon insertion of Pd(PEt₃)₂ into the carbon–halide bond. This effect may thus be independent of the coordination mode of the ligand (*normal* vs *abnormal*) or its partial charge (pyridylidene vs pyridyl). Computational studies support such a conclusion, since the σ and π orbital contributions in pyridyl–metal and pyridylidene–metal bonds have been calculated to be remarkably similar.²⁴

Consistent with our conclusions from crystallographic analyses, the observed influence of the metal fragment on the heterocycle might be rationalized by non-negligible M→L π -back-donation. In general, an essentially similar but stronger shielding/deshielding behavior is observed for the nickel(II) fragment compared to palladium(II).

(66) Pugmire, R. J.; Grant, D. M. *J. Am. Chem. Soc.* **1968**, *90*, 697.

(67) Tukov, A. A.; Normand, A. T.; Nechaev, M. S. *Dalton Trans.* **2009**, 7015.

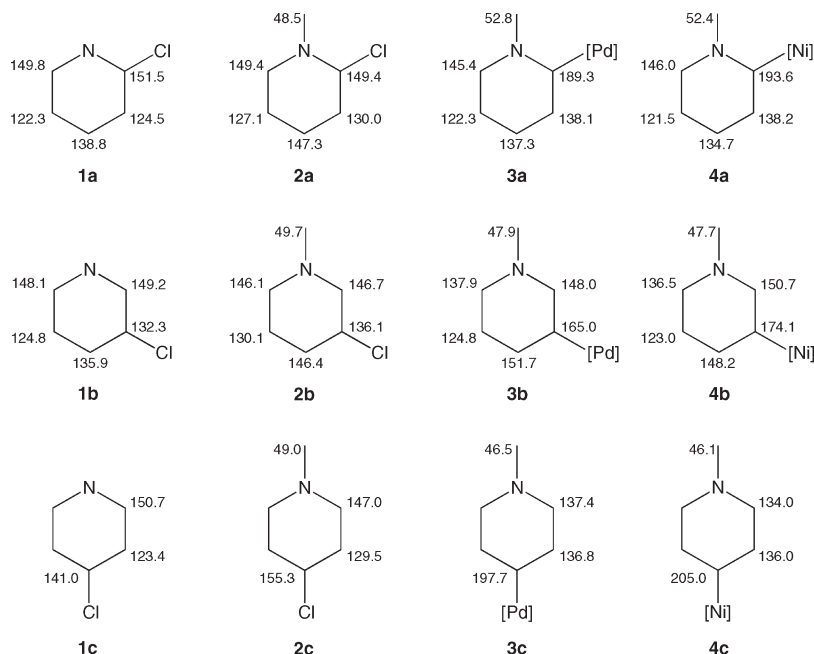


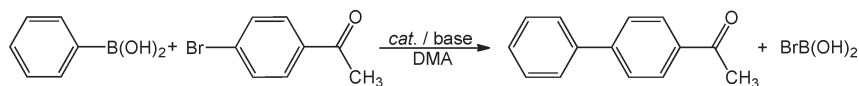
Figure 4. Summary of ^{13}C NMR chemical shifts in ppm.

Table 2. Computational Results at the BP86/TZ2P Level and Comparison with Experimental Values, Which Are Given in *Italics*^a

	$d(\text{M}-\text{C})$ [Å]	$d(\text{M}-\text{Cl})$ [Å]	CCX angle [deg]	E_{rel}^b [kcal mol ⁻¹]	E_{int}^c [kcal mol ⁻¹]
M3a	2.021 <i>2.002(3)</i>	2.342 <i>2.3638(8)</i>	116.23 <i>116.22</i>	0	-95.9
M3b	2.029 <i>1.996(7)</i>	2.347 <i>2.371(2)</i>	115.67 <i>117.82</i>	3.25	-105.9
M3c	2.019 <i>1.979(7)</i>	2.339 <i>2.3938(17)</i>	115.34 <i>114.64</i>	3.47	-109.3
M4a	1.873 <i>1.861(5)</i>	2.189 <i>2.203(1)</i>	116.10 <i>116.84</i>	0	-101.6
M4b	1.881 <i>1.874(3)</i>	2.192 <i>2.2055(8)</i>	115.47 <i>116.23</i>	3.61	-111.3
M4c	1.877 <i>1.863(5)</i>	2.179 <i>2.2172(13)</i>	115.13 <i>115.04</i>	3.72	-115.5

^a Compared to experimental values (cf. Table 1). ^b Relative minimized energies. ^c Metal-carbene interaction energies.

Scheme 4. Suzuki–Miyaura-Type Test Reactions



This effect may tentatively be assigned to a larger $\text{M}=\text{C}$ double-bond character in **4** than in the corresponding palladium complexes **3**.

Singlets in the ^{31}P NMR spectra of all complexes indicate the equivalence of both phosphine ligands, hence confirming a mutual *trans* arrangement also in solution (Scheme 2). Even though the resonances for complexes **3** and **4** fall in a narrow range (δ_{P} 22.7–24.9 and 21.2–23.0, respectively), both series show a common trend, i.e., 2- < 4- < 3-pyridylidene, suggesting an increasing donor strength of the carbene ligand in this order.⁶⁸

c. Computational Studies. Calculations for the series of isomeric palladium and nickel model complexes **M3** and **M4** comprising PH_3 ligands instead of PPh_3 (as in Scheme 2) were conducted at the BP86/TZ2P level of theory to verify and extend our interpretation of experimental results

(Table 2). The calculated $\text{M}-\text{C}$ bonds are slightly shorter than the experimental values, while the theoretical $\text{M}-\text{Cl}$ distances are a bit longer than the X-ray data, but the differences are not very large. The very small changes observed in the $\text{M}-\text{C}$ and $\text{M}-\text{Cl}$ bond lengths are within the error range of the theoretical and experimental data, and thus, they do not exhibit a significant trend. The theoretical and experimental CCX bond angles agree well. Also bond length variations within the rings, which were discussed in section b, are qualitatively reproduced. The calculated data of the model compounds may thus be used for the interpretation of the experimental results.

The relative energies of the model systems **M3** and **M4** follow the trend 2-pyridylidene << 3-pyridylidene < 4-pyridylidene, which is the same order that has been reported for the corresponding *free* carbene isomers of pyridine, in which one proton is located on the nitrogen atom.^{24,27,28} However, the energy differences are much smaller in the complexes and

(68) Iglesias, M.; Albrecht, M. *Dalton Trans.* **2010**, 39, 5213.

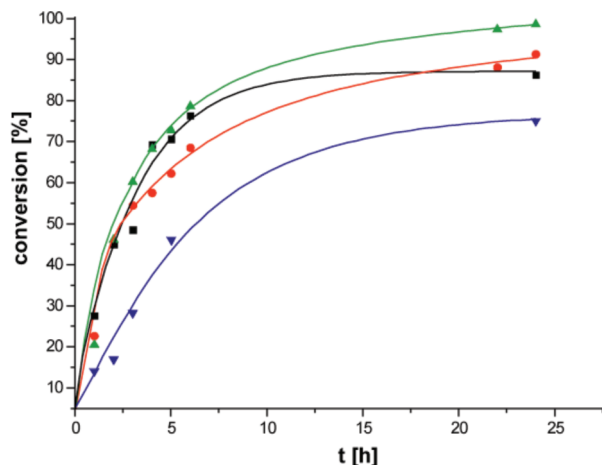
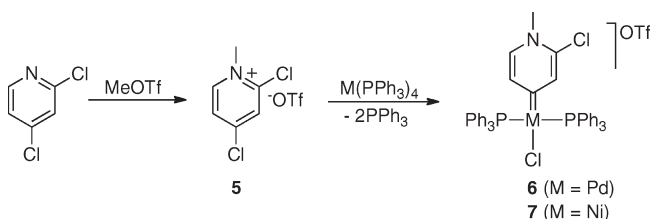


Figure 5. Time/conversion curves under inert conditions (**3a** squares; **3b** dots; **3c** triangles; Pd(PPh₃)₄ inverted triangles).

Scheme 5. Oxidative Addition in a Competitive Environment Yields Exclusively the 4-Pyridylidene Complexes **6 and **7****



can be rationalized by the calculated stronger interactions in 3- and 4-pyridylidene complexes, partly compensating the energy difference in the free pyridylidenes. The energy decomposition analysis of the metal–carbon bonds reveals increasing interaction energies (E_{int}) in the order 2-pyridylidene < 3-pyridylidene < 4-pyridylidene. In an extensive EDA study of pyridylidene and quinolylidene M–C bonds we could show that E_{int} correlates very well with the energy of the HOMO, i.e., the σ lone-pair orbital of the carbene and thus the σ -donor properties of a given ligand.²⁴

e. Catalysis. In order to determine the influence of abnormal and remote pyridylidene bonding modes on catalytic performance, the palladium complexes **3** were used in Suzuki–Miyaura cross-coupling reactions (Scheme 4).⁶⁹ Results of preliminary experiments under standard conditions indicated small but distinct differences in the catalytic activity. As a general trend, increasing remoteness enhanced the conversions, and yields of the biaryl product followed the trend **3c** (86%) > **3b** (82%) > **3a** (78%). All complexes displayed better performance than the reference complex Pd(PPh₃)₄ (71%). The trend was slightly more pronounced when using milder reaction temperatures and working under an inert atmosphere (Figure 5; also see Supporting Information).

No palladium black was observed during catalysis, thus suggesting a homogeneous mode of action. This assumption is further supported by the pertinent time–conversion profiles, which do not show any induction time or sigmoidal substrate conversion. Time-dependent monitoring also

(69) Test reactions under Buchwald–Hartwig conditions yielded palladium black even at very low temperatures, and no discrimination between the precatalysts **3** with Pd(OAc)₂ or PdCl₂ was possible, probably due to a predominantly heterogeneous mode of action.

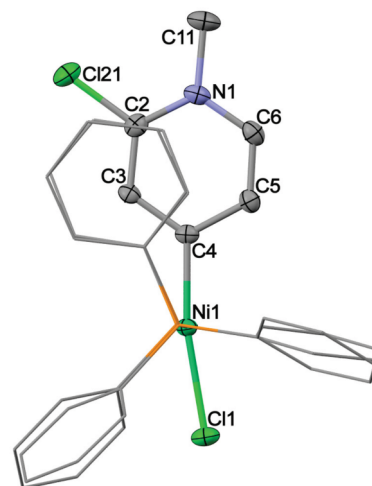


Figure 6. Molecular structure of **7** (50% probability ellipsoids, hydrogen atoms and counterion omitted). Selected bond lengths [Å] and angles [deg]: Ni1–C4 1.855(2), Ni1–C2 1.356(3), C2–C3 1.372(3), C3–C4 1.399(3), C4–C5 1.410(3), C5–C6 1.1359(3), C6–Ni1 1.355(3); C3–C4–C5 116.6(2), C4–Ni1–C11 170.24(7).

unveiled further subtle differences between the pyridylidene-based catalytic systems (Figure 5). The initial catalytic activity during the first two hours is very similar for all three complexes, perhaps slightly higher for the normal carbene complex **3a**. However, this complex seems to be the least robust and deactivates after extended periods of reaction time, thus not reaching high conversions. In contrast, the remote pyridylidene complexes **3b** and **3c** remain active even after 20 h of activity. Hence the general trends stated above need to be refined. While the *normal* pyridylidene complexes **3a** and **3c** are slightly more active than *abnormal* **3b**, the *remote* complexes **3c** and **3b** are more robust than **3a**. Since the differences observed here are only small, further tests will be needed in order to substantiate the deduced trends.

f. Regioselectivity of the Oxidative Addition of Pyridylum Salts. In addition to comparing the possible bonding modes of pyridylidenes, we were also interested in determining how carbene formation would preferentially occur when the metal complex reactant was presented with two active Cl-containing sites on the pyridinium ring. Reactions of M(PPh₃)₄ (M = Pd, Ni) with the dichlorinated methylpyridinium salt **5** in toluene (Scheme 5) yielded, according to ¹³C and ¹H NMR, exclusively the 4-pyridylidene complexes **6** and **7**. In comparison with the unsubstituted analogue **3c**, complex **6** shows a ca. 5 ppm downfield shift of the carbene resonance, which can be attributed to the *meta* influence of the chloride substituent. The ³¹P signals differ only insignificantly.

X-ray crystal structure determinations of **6** and **7** unambiguously confirmed the coordination sites deduced by NMR spectroscopy (Figure 6). The observed features are generally similar to those discussed above. Notably, the M–C distances of 1.972(4) and 1.855(2) Å for **6** and **7**, respectively, both represent the shortest bonds in the series of pyridylidene complexes discussed in this article. The M–Cl bonds are within the range described.

On the basis of the steric shielding effect of the N-methyl group in **5** and with reference to the seminal work by Carmona and co-workers,^{33,34,47} the observed regioselectivity of metalation might be ascribed to steric discrimination. However, the same selectivity was observed when the

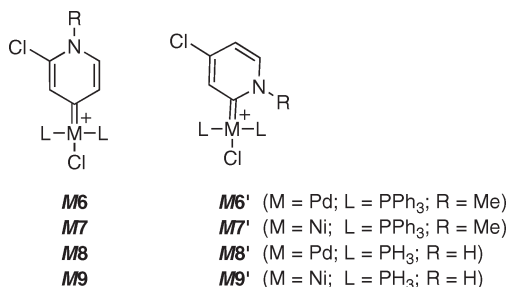


Figure 7. Models of the possible products formed upon oxidative addition in Scheme 5.

Table 3. Computational Results

	E_{rel}^a [kcal/mol]	E_{int}^b [kcal/mol]
M6 ^c	7.9	n/a
M6' ^c	0	n/a
M7 ^c	6.9	n/a
M7' ^c	0	n/a
M8 ^d	5.6	-103.1
M8' ^d	0	-91.0
M9 ^d	4.9	-109.3
M9' ^d	0	-96.6

^a Relative minimized energies. ^b Bond interaction energies. ^c BP86/TZVPP. ^d BP86/TZ2P.

protonated analogue of **5** was used as ligand precursor. While the palladium homologue of **6** could not be obtained in pure form, NMR spectra clearly indicated the formation of the C4-bound complex as the main product and the only carbene species (for details see Experimental Section). A good agreement with the signals in the spectra of **6** and especially ²J_{CP} couplings for two carbon atoms are indicative of the selective formation of the C4-bound isomer. Obviously, metalation of the remote 4-position is not sterically triggered but is electronically preferred.

The fact that metal attack occurs preferentially at the remote position can be understood against the background of established pyridine cross-coupling chemistry.⁷⁰ Although the aryl addition mechanism in such reactions is still a matter of debate, all proposed pathways (i.e., concerted, S_N2, free halide)^{71–73} feature the electron-rich d¹⁰ metal as a nucleophile. Accordingly, preferential attack at the most electron-deficient 2-position can be assumed and is indeed observed. For example 2,4-dibromopyridine is metalated by Pd(PPh₃)₄ almost exclusively in the *ortho* position.⁷⁴ This corresponds to the most deshielded carbon atom according to NMR results (C2: δ_C 142.5; C4: δ_C 133.9). In our case, where the precursor **5** features ¹³C carbon shifts of 148.9 and 156.0 ppm for C2 and C4, respectively, attack also occurs at the most deshielded (i.e., the presumably more electrophilic) site.

Calculation of the relative energies for realistic models of **6** and **7** (Figure 7) at the BP86/TZVPP level of theory revealed that the 2-pyridylidene complexes **M6'** and **M7'** are more stable than the 4-congeners **M6** and **M7** (E_{rel} in Table 3). The same trend was calculated for the 2- and 4-substituted isomers **M3a/M3c** and **M4a/M4c** (Table 2), which suggests that the relative stability of the 2- and 4-substituted systems

does not depend on the steric requirements of the ligand. We also calculated the computationally less demanding 4-substituted model compounds **M8/M9** and their 2-substituted congeners **M8'/M9'** and found a similar energy difference in favor of the latter isomers, as for the bulkier compounds (Table 3). Energy decomposition analysis on these simpler models further shows that the stronger interaction occurs in the *para* position (E_{int} in Table 3). These findings are consistent with the results shown in Table 2 and with our previous EDA studies on pyridylidenes.²⁴

The theoretically predicted higher stability of the 2-pyridylidene complexes **M6'** and **M7'** and the experimental finding that only the 4-congeners **6** and **7** are formed indicate that these less stable isomers are the products of a kinetically controlled reaction. This is a very important result, which we shall investigate in a future study. We do not think that the calculations predict a wrong stability order, because we obtain the same trend with similar energy differences using different models. Also, since the calculations involve different isomers of the same molecule, it can be expected that the results are quite reliable. A theoretical study of the reaction course is quite expensive because different pathways are possible. The theoretical work shall therefore be complemented by kinetic studies.

As an extension of our studies on quinolyldenies,^{20,21,23,40–42} we also compared the reactivity of M(PPh₃)₄ toward dichloroquinolinium salts **8** where both chloro substituents (Scheme 6) are three bonds removed from the methylated (R = Me) or protonated (R = H) nitrogen atom. Again, only one of the possible products was formed in each reaction. Consistent with the expected electrophilicity derived from the ¹³C NMR spectra of the precursors (C4: δ_C 155; C7: δ_C 144), metalation is preferred within the N-containing ring to yield complexes **9** and **10**. In comparison with the monocyclic congeners in **3c** and **4c**, the quinolylidene carbene signals are shifted about 10 ppm downfield, while the ³¹P NMR shifts remain essentially identical.

No traces of any dinuclear complexes were found even when using an excess of metal precursor. Figure 8 depicts the crystal structure of **9a**, indicating that the presence of bulky phosphine ligands excludes the formation of dinuclear products.

Conclusions

While X-ray structural data and ¹³C NMR measurements of the *normal* (both adjacent and *remote* to N) complexes within a complete set of pyridine-derived carbene complexes consistently support a carbenoid-type bonding (i.e., partial M=C double-bond character), results for the *abnormal* examples cannot be described in terms of simple valence bond resonance theory. However, close examination reveals a coherent and consistent influence of the metal fragments on the heterocyclic ligand in all bonding modes. Due to an apparent influence of *remote* carbene bonding on catalytic robustness, this concept seems slightly more relevant for catalytic application than the variation between *normal* and *abnormal* bonding situations. In an investigation of competitive carbene complex formation by oxidative insertion, *remote* 4-pyridylidene formation is favored over that of 2-pyridylidene formation even in the absence of steric shielding at nitrogen. Overall, we conclude that the concepts of *remote* and (*ab*)*normal* carbene bonding are useful and their

(70) Schroter, S.; Stock, C.; Bach, T. *Tetrahedron* **2005**, *61*, 2245.

(71) Fitton, P.; Rick, E. A. *J. Organomet. Chem.* **1971**, *28*, 287.

(72) Portnoy, M.; Milstein, D. *Organometallics* **1993**, *12*, 1665.

(73) Senn, H. M.; Ziegler, T. *Organometallics* **2004**, *23*, 2980.

(74) Sicre, C.; Alonso-Gomez, J.; Cid, M. M. *Tetrahedron* **2006**, *62*, 11063.

Scheme 6. Competitive Oxidative Addition at Dichloroquinolinium Salts

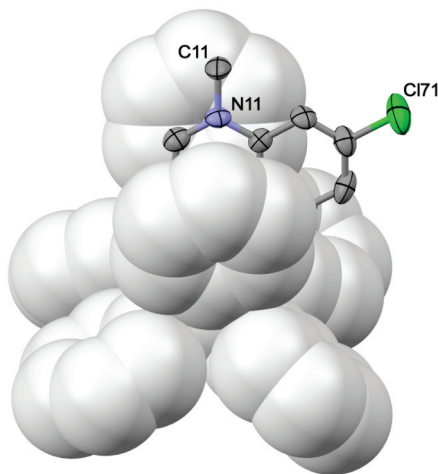
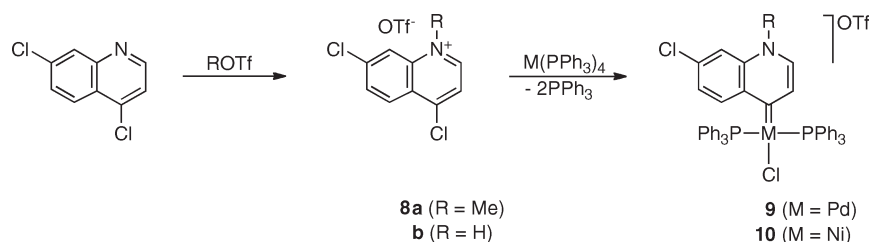


Figure 8. Occlusion of the quinolydene ligand by PPh₃ ligands in **9a**.

differences are well reflected in our experimental observations in various pyridylidene complexes of Pd and Ni.

Experimental Section

General Procedures. All manipulations were performed in a dry argon atmosphere using standard Schlenk techniques. Pd(PPh₃)₄⁷⁵ was prepared using a previously published method. All other chemicals were commercially available. Diethyl ether, hexane, and pentane were freshly distilled under N₂ from sodium wire and CH₂Cl₂ from CaH₂. Melting points (uncorrected) were determined on a Stuart SMP3 apparatus. NMR spectra were determined on a Varian 300 FT or INOVA 600 MHz spectrometer (¹H NMR at 300/600 MHz, ¹³C{¹H} NMR at 75/151 MHz, and ³¹P{¹H} NMR at 121.5/243 MHz). ¹H and ¹³C chemical shifts refer to δ_{TMS} = 0.00 according to the residual deuterated solvents and are reported in ppm. ³¹P chemical shifts are reported in ppm relative to an 85% H₃PO₄ external standard. FAB-MS determinations were performed on a VG 70SEQ mass spectrometer in a 2-nitrobenzyl alcohol matrix at the University of Witwatersrand, South Africa.

Procedure A: Preparation of Methylated Triflate Salts. A small excess (1.1 molar equiv) of methyl trifluoromethanesulfonate was added dropwise to a solution of the respective pyridine/quinoline precursor in 20 mL of CH₂Cl₂. The solution was stirred for 18 h at room temperature, after which the solvent was removed by cannula. The resulting precipitate was washed with ether (3 × 10 mL) and dried under high vacuum for a few hours.

For the synthesis of the 4-substituted salt, 4-chloropyridine·HCl (5.00 g, 33.3 mmol) was dissolved in 50 mL of distilled water, and 40 mL of 1 M NaOH was added. The aqueous solution was extracted with ether (3 × 40 mL). The organic

phase was washed with brine, dried with MgSO₄, and concentrated in a brown Schlenk tube. The oil (2.18 g, 19.2 mmol) was dissolved in CH₂Cl₂ and cooled to -78 °C, and methyl trifluoromethanesulfonate (3.46 g, 2.40 mL, 21.1 mmol) was added dropwise. The mixture was stirred overnight while it was allowed to warm to room temperature. The solvent was removed *in vacuo*, and the resulting product was washed once with 10 mL of THF and twice with 10 mL of diethyl ether.

Procedure B: Preparation of Protonated Triflate Salts. The hydropyridinium triflate salts were obtained by reacting the ligand precursor with a small excess (1.1 molar equiv) of CF₃SO₃H in 20 mL of CH₂Cl₂ at room temperature for 18 h. Diethyl ether (20 mL) was added and a white precipitate formed. The solvent was removed via a cannula and the resulting solid washed with 4 × 20 mL of diethyl ether and dried *in vacuo*.

Procedure C: Preparation of *trans*-Chloro(pyridylidene)bis-(triphenylphosphine)palladium(II) Triflate Complexes. The respective triflate salts and a small excess (1.01 molar equiv) of Pd(PPh₃)₄ were suspended in 30 mL of toluene and stirred for 17 h at 60 °C (in the case of **3b**, the reaction mixture was stirred for 64 h). The white suspension in a light yellow solution was allowed to cool to room temperature and filtered through Celite. The solid on the filter was washed with 4 × 5 mL of toluene, and the product was dissolved in CH₂Cl₂ and filtered, to yield after solvent evaporation *in vacuo* the microcrystalline palladium complexes.

Procedure D: Preparation of *trans*-Chloro(pyridylidene)bis-(triphenylphosphine)nickel(II) Triflate Complexes. A small excess (1.1 molar equiv) of Ni(PPh₃)₄ and the respective triflate salt were suspended in THF (20 mL), and the mixture was stirred at room temperature for 17 h. The resulting yellow precipitate in a brown solution was filtered through Celite and washed with 3 × 5 mL of toluene. The product was dissolved in CH₂Cl₂, filtered, and dried under high vacuum.

2-Chloro-1-methylpyridinium Triflate, 2a. According to procedure A: 88.0% yield of colorless microcrystalline material; mp 163.3–165.0 °C. ¹H NMR (CD₂Cl₂, 20 °C): δ 4.49 (3H, s, NMe), 8.02 (1H, m, H⁵), 8.06 (1H, dd, ³J = 8.3 Hz, ⁴J = 1.3 Hz, H³), 8.45 (1H, td, ³J = 8.3 Hz, ³J = 1.7 Hz, H⁴), 9.18 (1H, dd, ³J = 6.2 Hz, ³J = 1.7 Hz, H⁶). ¹³C{¹H} NMR (CD₂Cl₂, 20 °C): δ 48.5 (s, NMe), 127.1 (s, C⁵), 130.0 (s, C³), 147.3 (s, C⁴), 149.4 (bs, C² and C⁶), CF₃ not observed. Anal. Calcd for C₇H₇NO₃SClF₃ (277.65 g·mol⁻¹): C 30.28, H 2.54, N 5.04. Found: C 30.01, H 2.41, N 4.93.

3-Chloro-1-methylpyridinium triflate, 2b. According to procedure A: 98.5% yield of colorless microcrystalline material; mp 60.8–62.3 °C. ¹H NMR (CD₂Cl₂, 20 °C): δ 4.63 (3H, s, NMe), 8.29 (1H, dd, ³J = 8.3 Hz, ³J = 6.3 Hz, H⁵), 8.81 (1H, dm, ³J = 8.3 Hz, ⁴J = 0.5 Hz, H⁶), 9.15 (1H, d, ³J = 6.3 Hz, H⁴), 9.38 (1H, d, ⁴J = 0.5 Hz, H²). ¹³C{¹H} NMR (CD₂Cl₂, 20 °C): δ 49.7 (s, NMe), 130.1 (s, C⁵), 136.1 (s, C³), 146.1 (s, C⁶), 146.4 (s, C⁴), 146.7 (s, C²), CF₃ not observed. MS (FAB): *m/z* (%) 130.1 (35) [M - CF₃SO₃]⁺, (³⁷Cl); 128.1 (100) [M - CF₃SO₃]⁺, (³⁵Cl). Anal. Calcd for C₇H₇NO₃SClF₃ (277.65 g·mol⁻¹): C 30.28, H 2.54, N 5.04. Found: C 30.80, H 2.30, N 5.09.

4-Chloro-1-methylpyridinium triflate, 2c. According to procedure A: 55.5% yield of colorless microcrystalline material; mp 135.1–136.6 °C. ¹H NMR (CD₂Cl₂, 20 °C): δ 4.45 (3H, s, NMe),

(75) Ozawa, F. In *Synthesis of Organometallic Compounds*; Komiya, S., Ed.; John Wiley & Sons: Chichester, 1997.

8.01 (2H, d, $^3J = 6.8$ Hz, H³ and H⁵), 8.82 (2H, d, $^3J = 6.8$ Hz, H² and H⁶). $^{13}\text{C}\{^1\text{H}\}$ NMR (CD₂Cl₂, 20 °C): δ 49.0 (s, NMe), 129.5 (s, C³ and C⁵), 147.0 (bs, C² and C⁶), 155.3 (s, C⁴), CF₃ not observed. Anal. Calcd for C₇H₇NO₃SClF₃ (277.65 g·mol⁻¹): C 30.28, H 2.54, N 5.04. Found: C 30.01, H 2.61, N 5.11.

trans-Chloro(2-hydro-1-methyl-2-pyridylidene)bis(triphenylphosphine)palladium(II) Triflate, 3a. According to procedure C: 96.3% yield of colorless microcrystalline material; mp (dec): 248 °C. ¹H NMR (CD₂Cl₂, 20 °C): δ 3.96 (3H, s, NMe), 7.00 (2H, m, H⁴ and H⁵), 7.40, 7.52 (31H, m, PPh with obscured H⁶), 7.89 (1H, d, $^3J = 6.0$ Hz, H³). $^{13}\text{C}\{^1\text{H}\}$ NMR (CD₂Cl₂, 20 °C): δ 52.8 (s, NMe), 122.3 (s, C⁵), 128.9 (m, PPh^{ipso}), 129.3 (m, PPh^{meta}), 131.8 (s, PPh^{para}), 134.3 (m, PPh^{ortho}), 137.3 (s, C⁴), 138.1 (t, $^3J_{\text{C-P}} = 3.9$ Hz, C³), 145.4 (s, C⁶), 189.3 (t, $^2J_{\text{C-P}} = 6.5$ Hz, C²), CF₃ not observed. $^{31}\text{P}\{^1\text{H}\}$ NMR (CD₂Cl₂, 20 °C): δ 22.7 (s, PPh₃). Anal. Calcd for C₄₃H₃₇NO₃P₂SClF₃Pd (908.64 g·mol⁻¹): C 56.84, H 4.10, N 1.54. Found: C 57.03, H 4.19, N 1.60.

trans-Chloro(3-hydro-1-methyl-3-pyridylidene)bis(triphenylphosphine)palladium(II) Triflate, 3b. According to procedure C: 90.8% yield of colorless crystals; mp (dec): 195 °C. Single crystals suitable for structure determination were obtained by dissolving the crude mixture in CH₂Cl₂ and allowing pentane to diffuse slowly into the mixture at -20 °C. ¹H NMR (CD₂Cl₂, 20 °C): δ 3.54 (3H, s, NMe), 6.73 (1H, dd, $^3J = 7.7$ Hz, $^3J = 6.0$ Hz, H⁵), 7.26 (1H, bs, H²), 7.40, 7.49, 7.58 (30H, m, PPh), 7.78 (1H, d, $^3J = 7.7$ Hz, H⁴), 7.82 (1H, d, $^3J = 6.0$ Hz, H⁶). $^{13}\text{C}\{^1\text{H}\}$ NMR (CD₂Cl₂, 20 °C): δ 47.9 (s, NMe), 124.8 (s, C⁵), 129.0 (m, PPh^{ipso}), 129.4 (m, PPh^{meta}), 131.4 (s, PPh^{para}), 134.8 (m, PPh^{ortho}), 137.9 (s, C⁶), 148.0 (t, $^3J_{\text{CP}} = 4.9$ Hz, C²), 151.7 (t, $^3J_{\text{CP}} = 3.5$ Hz, C⁴), 165.0 (t, $^2J_{\text{CP}} = 6.9$ Hz, C³), CF₃ not observed. $^{31}\text{P}\{^1\text{H}\}$ NMR (CD₂Cl₂, 20 °C): δ 24.9 (s, PPh₃). MS (FAB): m/z (%) 759.6 (52) [M - CF₃SO₃]⁺, (³⁵Cl, ¹⁰⁶Pd); 498.0 (66) [M - PPh₃ - CF₃SO₃]⁺; 460.1 (21) [M - PPh₃ - Cl - CF₃SO₃]⁺; 384.7 (10) [M - 2PPh₃ - Cl - CF₃SO₃]⁺. Anal. Calcd for C₄₃H₃₇NO₃P₂SClF₃Pd (908.64 g·mol⁻¹): C 56.84, H 4.10, N 1.54. Found: C 56.99, H 4.01, N 1.60.

trans-Chloro(4-hydro-1-methyl-4-pyridylidene)bis(triphenylphosphine)palladium(II) Triflate, 3c. According to procedure C: 99% yield of colorless microcrystalline material; mp (dec) 189 °C. ¹H NMR (CD₂Cl₂, 20 °C): δ 3.80 (3H, s, NMe), 7.16 (2H, d, $^3J = 6.4$ Hz, H² and H⁶), 7.39 (14H, m, PPh with obscured H³ and H⁵), 7.50, 7.62 (18H, m, PPh). $^{13}\text{C}\{^1\text{H}\}$ NMR (CD₂Cl₂, 20 °C): δ 46.5 (s, NMe), 129.2 (m, PPh^{meta}), 130.0 (m, PPh^{ipso}), 131.7 (s, PPh^{para}), 135.2 (m, PPh^{ortho}), 136.8 (bs, C³ and C⁵), 137.4 (s, C² and C⁶), 197.7 (t, $^2J = 6.5$ Hz, C⁴), CF₃ not observed. $^{31}\text{P}\{^1\text{H}\}$ NMR (CD₂Cl₂, 20 °C): δ 23.6 (s, PPh₃). Anal. Calcd for C₄₃H₃₇NO₃P₂SClF₃Pd (908.64 g·mol⁻¹): C 56.84, H 4.10, N 1.54. Found: C 56.61, H 3.98, N 1.59.

trans-Chloro(2-hydro-1-methyl-2-pyridylidene)bis(triphenylphosphine)nickel(II) Triflate, 4a. According to procedure D: 58.9% yield of yellow microcrystalline material; mp (dec) 187 °C. ¹H NMR (CD₂Cl₂, 20 °C): δ 4.22 (3H, s, NMe), 6.81 (1H, m, H⁵), 6.91 (1H, td, $^3J = 7.7$ Hz, $^4J = 1.4$ Hz, H⁴), 7.42, 7.57 (31H, m, PPh with obscured H⁶), 7.85 (1H, m, H³). $^{13}\text{C}\{^1\text{H}\}$ NMR (CD₂Cl₂, 20 °C): δ 52.4 (s, NMe), 121.5 (s, C⁵), 128.9 (m, PPh^{ipso}), 129.4 (m, PPh^{meta}), 131.8 (s, PPh^{para}), 134.5 (m, PPh^{ortho}), 134.7 (s, C⁴), 138.2 (bs, C³), 146.0 (s, C⁶), 193.6 (t, $^3J_{\text{CP}} = 33.0$ Hz, C²), CF₃ not observed. $^{31}\text{P}\{^1\text{H}\}$ NMR (CD₂Cl₂, 20 °C): δ 21.2 (s, PPh₃). Anal. Calcd for C₄₃H₃₇NO₃P₂SClF₃Ni (860.91 g·mol⁻¹): C 59.99, H 4.33, N 1.63. Found: C 60.32, H 4.24, N 1.49.

trans-Chloro(3-hydro-1-methyl-3-pyridylidene)bis(triphenylphosphine)nickel(II) Triflate, 4b. According to procedure D: 49.6% yield of light yellow crystals; mp (dec) 135.0–138.0 °C. Yellow crystals, suitable for single-crystal X-ray structure determination, were obtained by slow diffusion of pentane into a concentrated CH₂Cl₂ solution at -20 °C. ¹H NMR (CD₂Cl₂, 20 °C): δ 3.36 (3H, s, NMe), 6.69 (1H, m, H⁵), 7.11 (1H, bs, H⁴), 7.40, 7.66 (31H, m, PPh with obscured H⁶), 8.09 (1H, d, $^4J = 4.4$ Hz, H²). $^{13}\text{C}\{^1\text{H}\}$ NMR (CD₂Cl₂, 20 °C): δ 47.7 (s, NMe), 123.0 (s, C⁵), 128.9 (m, PPh^{meta}), 129.7 (m, PPh^{ipso}), 131.2 (s, PPh^{para}), 134.7 (m, PPh^{ortho}), 136.5 (s, C⁶), 148.2 (s, C⁴), 150.7 (bs, C²), 174.1 (bs, C³), CF₃ not

observed. $^{31}\text{P}\{^1\text{H}\}$ NMR (CD₂Cl₂, 20 °C): δ 23.0 (s, PPh₃). MS (FAB): m/z (%) 711.8 (8) [M - CF₃SO₃]⁺, (³⁷Cl, ⁵⁸Ni); 449.6 (70) [M - PPh₃ - CF₃SO₃]⁺; 413.0 (24) [M - PPh₃ - Cl - CF₃SO₃]⁺. Anal. Calcd for C₄₃H₃₇NO₃P₂SClF₃Ni (860.91 g·mol⁻¹): C 59.99, H 4.33, N 1.63. Found: C 60.21; H 4.20; N 1.73.

trans-Chloro(4-hydro-1-methyl-4-pyridylidene)bis(triphenylphosphine)nickel(II) Triflate, 4c. According to procedure D: 45.7% yield of yellow microcrystalline material; mp (dec) 153 °C. ¹H NMR (CD₂Cl₂, 20 °C): δ 3.70 (3H, s, NMe), 6.91 (2H, d, $^3J = 5.9$ Hz, H² and H⁶), 7.40, 7.49, 7.68 (32H, m, PPh with obscured H³ and H⁵). $^{13}\text{C}\{^1\text{H}\}$ NMR (CD₂Cl₂, 20 °C): δ 46.1 (s, NMe), 128.8 (m, PPh^{meta}), 129.7 (m, PPh^{ipso}), 131.2 (s, PPh^{para}), 134.0 (s, C² and C⁶), 134.7 (m, PPh^{ortho}), 136.0 (bs, C³ and C⁵), 205.0 (t, $^3J = 31.2$ Hz, C⁴), CF₃ not observed. $^{31}\text{P}\{^1\text{H}\}$ NMR (CD₂Cl₂, 20 °C): δ 22.4 (s, PPh₃). Anal. Calcd for C₄₃H₃₇NO₃P₂SClF₃Ni (860.91 g·mol⁻¹): C 59.99, H 4.33, N 1.63. Found: C 60.21; H 4.23, N 1.54.

2,4-Dichloro-1-methylpyridinium Triflate, 5. According to procedure A: 99.8% yield of colorless microcrystalline material; mp 95.8–97.7 °C. ¹H NMR (CD₂Cl₂, 20 °C): δ 4.42 (3H, s, NMe), 7.99 (1H, dd, $^3J = 6.8$ Hz, $^4J = 2.3$ Hz, H⁵), 8.05 (1H, d, $^4J = 2.3$ Hz, H³), 9.14 (1H, dd, $^3J = 6.8$ Hz, $^5J = 0.4$ Hz, H⁶). $^{13}\text{C}\{^1\text{H}\}$ NMR (CD₂Cl₂, 20 °C): δ 48.1 (s, NMe), 127.7 (s, C⁵), 130.1 (s, C³), 148.9 (s, C⁴), 150.0 (s, C⁶), 156.0 (s, C²), CF₃ not observed. MS (FAB): m/z (%) 163.0 (77) [M - CF₃SO₃]⁺, (³⁷Cl); 161.9 (100) [M - CF₃SO₃]⁺, (³⁵Cl). Anal. Calcd for C₇H₆NO₃SCl₂F₃ (312.09 g·mol⁻¹): C 26.94, H 1.94, N 4.49. Found: C 26.88, H 1.99, N 4.57.

2,4-Dichloro-1-hydropyridinium Triflate. According to procedure B: 85.7% yield of colorless hygroscopic microcrystalline material; mp 115.4–117.0 °C. ¹H NMR (CD₂Cl₂, 20 °C): δ 7.94 (2H, m, H³ and H⁵), 8.79 (1H, m, H⁶), NH not observed. $^{13}\text{C}\{^1\text{H}\}$ NMR (CD₂Cl₂, 20 °C): δ 126.8 (s, C⁵), 128.7 (s, C³), 144.7 (s, C⁶), 146.6 (s, C²), 157.0 (s, C⁴), CF₃ not observed. MS (FAB): m/z (%) 147.9 (100) [M - CF₃SO₃]⁺, (³⁵Cl). Anal. Calcd for C₆H₄NO₃SCl₂F₃ (298.07 g·mol⁻¹): C 24.18, H 1.35, N 4.70. Found: C 23.29, H 1.41, N 4.54.

trans-Chloro(2-chloro-4-hydro-1-methyl-4-pyridylidene)bis(triphenylphosphine)palladium(II) Triflate, 6. According to procedure C: 74.3% yield of colorless crystals; mp (dec) 200 °C. ¹H NMR (CD₂Cl₂, 20 °C): δ 3.82 (3H, s, NMe), 7.16 (1H, bs, H³), 7.41 (12H, m, PPh^{meta}), 7.49 (7H, m, PPh^{para} with obscured H⁵), 7.63 (12H, m, PPh^{ortho}), 7.69 (1H, d, $^3J = 6.4$ Hz, H⁶). $^{13}\text{C}\{^1\text{H}\}$ NMR (CD₂Cl₂, 20 °C): δ 45.4 (s, NMe), 128.9 (m, PPh^{meta}), 129.3 (m, PPh^{ipso}), 131.5 (s, PPh^{para}), 134.6 (t, $^3J_{\text{CP}} = 3.7$ Hz, C⁵), 134.8 (m, PPh^{ortho}), 136.7 (t, $^3J_{\text{CP}} = 3.7$ Hz, C³), 139.2 (s, C²), 140.0 (s, C⁶), 202.3 (t, $^2J_{\text{CP}} = 6.1$ Hz, C⁴), CF₃ not observed. $^{31}\text{P}\{^1\text{H}\}$ NMR (CD₂Cl₂, 20 °C): δ 23.6 (s, PPh₃). MS (FAB): m/z (%) 794.0 (41) [M - CF₃SO₃]⁺, (³⁵Cl, ¹⁰⁶Pd); 758.6 (4) [M - Cl - CF₃SO₃]⁺; 531.9 (46) [M - PPh₃ - CF₃SO₃]⁺; 496.2 (8) [M - Cl - PPh₃ - CF₃SO₃]⁺. Anal. Calcd for C₄₃H₃₆NO₃P₂SCl₂F₃Pd (943.09 g·mol⁻¹): C 54.76; H 3.85; N 1.49. Found: C 54.57; H 3.78; N 1.55.

trans-Chloro(2-chloro-1,4-dihydro-4-pyridylidene)bis(triphenylphosphine)palladium(II) Triflate. According to procedure C: No pure material could be obtained. NMR signals of the main product are overlapping with signals from impurities; thus shifts were unequivocally assigned by gHSQC and gHMQC measurements. ¹H NMR (CD₂Cl₂, 20 °C): δ 7.15 (s, H³), 7.18 (H⁶), 7.37 (H⁵), 7.41 (m, PPh^{meta}), 7.50 (m, PPh^{para}), 7.63 (m, PPh^{ortho}), NH not observed. $^{13}\text{C}\{^1\text{H}\}$ NMR (CD₂Cl₂, 20 °C): δ 128.9 (m, PPh^{meta}), 129.2 (m, PPh^{ipso}), 131.7 (s, PPh^{para}), 133.2 (t, $^3J_{\text{CP}} = 3.6$ Hz, C⁵), 134.6 (s, C⁶), 134.7 (m, PPh^{ortho}), 135.3 (t, $^3J_{\text{CP}} = 4.3$ Hz, C³), 137.4 (s, C²), 204.6 (t, $^2J_{\text{CP}} = 6.1$ Hz, C⁴), CF₃ not observed. $^{31}\text{P}\{^1\text{H}\}$ NMR (CD₂Cl₂, 20 °C): δ 24.0 (s, PPh₃). MS (FAB): m/z (%) 780.3 (6) [M - CF₃SO₃]⁺, (³⁵Cl, ¹⁰⁶Pd); 744.5 (3) [M - Cl - CF₃SO₃]⁺; 482.2 (15) [M - Cl - PPh₃ - CF₃SO₃]⁺; 446.2 (3) [M - 2Cl - PPh₃ - CF₃SO₃]⁺.

trans-Chloro(2-chloro-4-hydro-1-methyl-4-pyridylidene)bis(triphenylphosphine)nickel(II) Triflate, 7. According to procedure D: 62.4% yield of yellow crystals; mp (dec) 160 °C.

^1H NMR (CD_2Cl_2 , 20 °C): δ 3.71 (3H, s, NMe), 7.16 (1H, bs, H^3), 7.41 (12H, m, PPh^{meta}), 7.48 (7H, m, PPh^{para} with obscured H^6), 7.69 (12H, m, $\text{PPh}^{\text{ortho}}$), 7.76 (1H, d, $^3J = 6.4$ Hz, H^5). $^{13}\text{C}\{^1\text{H}\}$ NMR (CD_2Cl_2 , 20 °C): δ 45.0 (s, NMe), 128.9 (m, PPh^{meta}), 129.4 (m, PPh^{ipso}), 131.5 (s, PPh^{para}), 133.8 (s, C^5), 134.7 (m, $\text{PPh}^{\text{ortho}}$), 136.6 (s, C^3), 136.8 (s, C^6), 136.9 (s, C^2), 210.8 (s, C^4), CF_3 not observed. $^{31}\text{P}\{^1\text{H}\}$ NMR (CD_2Cl_2 , 20 °C): δ 22.5 (s, PPh_3). MS (FAB): m/z (%) 746.3 (40) $[\text{M} - \text{CF}_3\text{SO}_3]^+$, (^{35}Cl , ^{58}Ni); 710.8 (9) $[\text{M} - \text{Cl} - \text{CF}_3\text{SO}_3]^+$; 484.0 (12) $[\text{M} - \text{PPh}_3 - \text{CF}_3\text{SO}_3]^+$. Anal. Calcd for $\text{C}_{43}\text{H}_{36}\text{NO}_3\text{P}_2\text{SCl}_2\text{F}_3\text{Ni}$ (895.36 $\text{g}\cdot\text{mol}^{-1}$): C 57.68; H 4.05; N 1.56. Found: C 57.45; H 4.20; N 1.49.

4,7-Dichloro-1-methylquinolinium Triflate, 8a. According to procedure A: 99.0% yield of colorless microcrystalline material; mp 108–111 °C. ^1H NMR (CD_2Cl_2 , 20 °C): δ 4.65 (3H, s, NMe), 8.03 (1H, dd, $^3J = 9.0$ Hz, $^4J = 1.8$ Hz, H^6), 8.12 (1H, d, $^3J = 6.5$ Hz, H^3), 8.36 (1H, d, $^4J = 1.8$ Hz, H^8), 8.56 (1H, d, $^3J = 9.0$ Hz, H^5), 9.44 (1H, d, $^3J = 6.5$ Hz, H^2). $^{13}\text{C}\{^1\text{H}\}$ NMR (CD_2Cl_2 , 20 °C): δ 46.4 (s, NMe), 119.1 (s, C^8), 123.2 (s, C^3), 126.8 (s, C^{10}), 128.7 (s, C^5), 132.7 (s, C^6), 139.9 (s, C^9), 144.4 (s, C^7), 151.2 (s, C^2), 154.6 (s, C^4), CF_3 not observed. MS (FAB): m/z (%) 214.0 (69) $[\text{M} - \text{CF}_3\text{SO}_3]^+$, (^{37}Cl); 212.0 (100) $[\text{M} - \text{CF}_3\text{SO}_3]^+$, (^{35}Cl). Anal. Calcd for $\text{C}_{11}\text{H}_8\text{NO}_3\text{SCl}_2\text{F}_3$ (362.15 $\text{g}\cdot\text{mol}^{-1}$): C 36.48, H 2.23, N 3.87. Found: C 36.26, H 2.29, N 3.78.

4,7-Dichloro-1-hydroquinolinium Triflate, 8b. According to procedure B: 98.0% yield of colorless microcrystalline material; mp 146.4–147.2 °C. ^1H NMR (CD_2Cl_2 , 20 °C): δ 8.00 (1H, dd, $^3J = 9.0$ Hz, $^4J = 2.0$ Hz, H^6), 8.08 (1H, d, $^3J = 6.0$ Hz, H^3), 8.47 (2H, m, H^5 and H^8), 9.10 (1H, d, $^3J = 6.0$ Hz, H^2), not observed NH. $^{13}\text{C}\{^1\text{H}\}$ NMR (CD_2Cl_2 , 20 °C): δ 121.3 (s, C^8), 122.8 (s, C^3), 126.4 (s, C^{10}), 127.3 (s, C^5), 133.2 (s, C^6), 139.1 (s, C^9), 143.9 (s, C^7), 155.1 (s, C^2), 145.1 (s, C^4), CF_3 not observed. MS (FAB): m/z (%) 198.0 (100) $[\text{M} - \text{H} - \text{CF}_3\text{SO}_3]^+$, (^{35}Cl). Anal. Calcd for $\text{C}_{10}\text{H}_6\text{NO}_3\text{SCl}_2\text{F}_3$ (348.13 $\text{g}\cdot\text{mol}^{-1}$): C 34.50, H 1.74, N 4.02. Found: C 34.28, H 1.81, N 4.12.

trans-Chloro(7-chloro-4-hydro-1-methyl-4-quinolydene) bis(triphenylphosphine)palladium(II) Triflate, 9a. According to procedure C: 62.9% yield of colorless crystals; mp (dec) 204 °C. ^1H NMR (CD_2Cl_2 , 20 °C): δ 4.03 (3H, s, NMe), 7.28 (12H, m, PPh^{meta}), 7.40 (6H, m, PPh^{para}), 7.54 (14H, m, $\text{PPh}^{\text{ortho}}$ with obscured H^6 and H^8), 7.64 (1H, d, $^3J = 6.4$ Hz, H^3), 7.95 (1H, d, $^3J = 6.4$ Hz, H^5), 8.74 (1H, d, $^3J = 8.8$ Hz, H^2). $^{13}\text{C}\{^1\text{H}\}$ NMR (CD_2Cl_2 , 20 °C): δ 43.5 (s, NMe), 117.2 (s, C^8), 128.7 (m, PPh^{meta}), 129.3 (m, PPh^{ipso} with C^6), 130.6 (t, $^3J_{\text{CP}} = 3.6$ Hz, C^3), 131.4 (s, PPh^{para}), 134.5 (bs, C^{10}), 134.6 (m, $\text{PPh}^{\text{ortho}}$), 135.1 (s, C^9), 137.0 (s, C^5), 141.2 (s, C^7), 141.8 (s, C^2), 206.6 (t, $^2J_{\text{CP}} = 5.5$ Hz, C^4), CF_3 not observed. $^{31}\text{P}\{^1\text{H}\}$ NMR (CD_2Cl_2 , 20 °C): δ 23.2 (s, PPh_3). MS (FAB): m/z (%) 844.0 (74) $[\text{M} - \text{CF}_3\text{SO}_3]^+$, (^{35}Cl , ^{106}Pd); 581.9 (100) $[\text{M} - \text{PPh}_3 - \text{CF}_3\text{SO}_3]^+$; 546.0 (13) $[\text{M} - \text{Cl} - \text{PPh}_3 - \text{CF}_3\text{SO}_3]^+$; 404.1 (54) $[\text{M} - \text{L} - \text{PPh}_3 - \text{CF}_3\text{SO}_3]^+$. Anal. Calcd for $\text{C}_{47}\text{H}_{38}\text{NO}_3\text{P}_2\text{SCl}_2\text{F}_3\text{Pd}$ (993.14 $\text{g}\cdot\text{mol}^{-1}$): C 56.84; H 3.86; N 1.41. Found: C 56.66; H 3.99; N 1.32.

trans-Chloro(7-chloro-1,4-dihydro-4-quinolydene)bis(triphenylphosphine)palladium(II) Triflate, 9b. According to procedure C: 85.3% yield of colorless microcrystalline material; mp (dec) 207 °C. ^1H NMR (CD_2Cl_2 , 20 °C): δ 7.27 (12H, m, PPh), 7.41 (6H, m, PPh), 7.43 (1H, dd, $^3J = 8.8$ Hz, $^4J = 2.0$ Hz, H^6), 7.49 (1H, d, $^3J = 5.8$ Hz, H^2), 7.52 (13H, m, PPh with obscured H^3), 7.69 (1H, d, $^4J = 2.0$ Hz, H^8), 8.55 (1H, d, $^3J = 8.8$ Hz, H^5), not observed NH. $^{13}\text{C}\{^1\text{H}\}$ NMR (CD_2Cl_2 , 20 °C): δ 120.2 (s, C^8), 128.7 (m, PPh^{meta}), 129.2 (m, PPh^{ipso}), 129.3 (s, C^9), 129.4 (s, C^6), 129.6 (t, $^3J_{\text{CP}} = 4.3$ Hz, C^3), 131.5 (s, PPh^{para}), 133.8 (t, $^3J_{\text{CP}} = 2.5$ Hz, C^{10}), 134.5 (m, $\text{PPh}^{\text{ortho}}$), 135.2 (s, C^5), 135.6 (s, C^2), 140.2 (s, C^7), 207.2 (t, $^2J_{\text{CP}} = 5.5$ Hz, C^4), CF_3 not observed. $^{31}\text{P}\{^1\text{H}\}$ NMR (CD_2Cl_2 , 20 °C): δ 23.8 (s, PPh_3). MS (FAB): m/z (%) 830.4 (5) $[\text{M} - \text{CF}_3\text{SO}_3]^+$, (^{35}Cl , ^{106}Pd); 794.5 (1) $[\text{M} - \text{Cl} - \text{CF}_3\text{SO}_3]^+$; 568.3 (5) $[\text{M} - \text{PPh}_3 - \text{CF}_3\text{SO}_3]^+$; 532.3 (1) $[\text{M} - \text{Cl} - \text{PPh}_3 - \text{CF}_3\text{SO}_3]^+$. Anal. Calcd for $\text{C}_{46}\text{H}_{36}\text{NO}_3\text{P}_2\text{SCl}_2\text{F}_3\text{Pd}$ (979.12 $\text{g}\cdot\text{mol}^{-1}$): C 56.43, H 3.71, N 1.43. Found: C 56.22, H 3.87, N 1.46.

trans-Chloro(7-chloro-4-hydro-1-methyl-4-quinolydene)bis(triphenylphosphine)nickel(II) Triflate, 10a. According to procedure D: 80.4% yield of yellow crystals; mp (dec) 176 °C. ^1H NMR (CD_2Cl_2 , 20 °C): δ 3.90 (3H, s, NMe), 7.29 (12H, m, PPh^{meta}), 7.42 (7H, m, PPh^{para} with obscured H^8), 7.59 (13H, m, $\text{PPh}^{\text{ortho}}$ with obscured H^6), 7.66 (1H, d, $^3J = 6.3$ Hz, H^3), 7.89 (1H, d, $^3J = 6.3$ Hz, H^5), 9.44 (1H, d, $^3J = 8.8$ Hz, H^2). $^{13}\text{C}\{^1\text{H}\}$ NMR (CD_2Cl_2 , 20 °C): δ 43.0 (s, NMe), 117.2 (s, C^8), 128.6 (m, PPh^{meta}), 128.8 (s, C^6), 129.3 (m, PPh^{ipso}), 130.6 (bs, C^3), 131.2 (s, PPh^{para}), 133.3 (s, C^9), 134.6 (m, $\text{PPh}^{\text{ortho}}$), 135.3 (s, C^{10}), 136.6 (s, C^5), 137.9 (s, C^2), 140.9 (s, C^7), 216.7 (t, $^2J_{\text{CP}} = 30.5$ Hz, C^4), CF_3 not observed. $^{31}\text{P}\{^1\text{H}\}$ NMR (CD_2Cl_2 , 20 °C): δ 21.9 (s, PPh_3). MS (FAB): m/z (%) 796.2 (19) $[\text{M} - \text{CF}_3\text{SO}_3]^+$, (^{35}Cl , ^{58}Ni); 533.9 (68) $[\text{M} - \text{PPh}_3 - \text{CF}_3\text{SO}_3]^+$. Anal. Calcd for $\text{C}_{47}\text{H}_{38}\text{NO}_3\text{P}_2\text{SCl}_2\text{F}_3\text{Ni}$ (945.42 $\text{g}\cdot\text{mol}^{-1}$): C 59.71; H 4.05; N 1.48. Found: C 60.07; H 4.26; N 1.39.

trans-Chloro(7-chloro-1,4-dihydro-4-quinolydene)bis(triphenylphosphine)nickel(II) Triflate, 10b. According to procedure D: 68.1% yield of yellow crystals; mp (dec) 197 °C. ^1H NMR (CD_2Cl_2 , 20 °C): δ 7.28 (13H, m, PPh with obscured H^3), 7.40 (6H, m, PPh), 7.48 (1H, dd, $^3J = 8.8$ Hz, $^4J = 1.9$ Hz, H^6), 7.55 (13H, m, PPh with obscured H^8), 7.77 (1H, d, $^3J = 5.8$ Hz, H^2), 9.19 (1H, d, $^3J = 8.8$ Hz, H^5), not observed NH. $^{13}\text{C}\{^1\text{H}\}$ NMR (CD_2Cl_2 , 20 °C): δ 120.3 (s, C^8), 128.6 (m, PPh^{meta}), 128.7 (s, C^6), 129.3 (m, PPh^{ipso}), 129.6 (t, $^3J_{\text{CP}} = 3.7$ Hz, C^3), 131.3 (s, PPh^{para}), 132.0 (s, C^2), 132.0 (s, C^9), 134.4 (m, $\text{PPh}^{\text{ortho}}$), 134.7 (bs, C^{10}), 134.9 (s, C^5), 140.0 (s, C^7), 216.6 (t, $^2J_{\text{CP}} = 30.0$ Hz, C^4), CF_3 not observed. $^{31}\text{P}\{^1\text{H}\}$ NMR (CD_2Cl_2 , 20 °C): δ 22.6 (s, PPh_3). MS (FAB): m/z (%) 782.1 (3) $[\text{M} - \text{CF}_3\text{SO}_3]^+$, (^{35}Cl , ^{58}Ni); 746.9 (1) $[\text{M} - \text{Cl} - \text{CF}_3\text{SO}_3]^+$; 520.0 (10) $[\text{M} - \text{Cl} - \text{PPh}_3 - \text{CF}_3\text{SO}_3]^+$. Anal. Calcd for $\text{C}_{46}\text{H}_{36}\text{NO}_3\text{P}_2\text{SCl}_2\text{F}_3\text{Ni}$ (931.39 $\text{g}\cdot\text{mol}^{-1}$): C 59.32, H 3.90, N 1.50. Found: C 59.11, H 4.02, N 1.63.

Typical Procedure for the Suzuki–Miyaura Coupling. The reactions were performed under inert conditions using dry and degassed reagents. Phenylboronic acid (3 mmol, 0.3658 g), bromoacetophenone (2 mmol, 0.3981 g), potassium carbonate/cesium carbonate (4 mmol, 0.5528/1.303 g), diethyleneglycol-*n*-butyl ether (2 mmol, 0.4367 g, 0.5 mL), and dimethylacetamide (5 mL) were placed in a 25 mL three-neck round-bottom flask. The flask was connected to N_2 and equipped with a reflux condenser and a septum. The catalyst solution was added after heating to 130 °C. Aliquots (0.2 mL) were taken at regular intervals from the reaction mixture and added to 5 mL of CH_2Cl_2 . The organic layer was washed with 3×5 mL of water, dried over MgSO_4 , and filtered. The solvent was removed *in vacuo*, and the residue was analyzed by ^1H NMR spectroscopy.

Crystal Structure Determinations. Data associated with the crystal structures are summarized in Tables 4 and 1S, Supporting Information. Intensity data were collected at $T = 100$ K with a Bruker SMART Apex diffractometer with graphite-monochromated Mo $\text{K}\alpha$ radiation ($\lambda = 0.71073$ Å). Intensities were measured using the ω -scan mode and were corrected for Lorentz and polarization effects.^{76–79} The structures were solved by direct methods (SHELXS-97) and refined by full-matrix least-squares on F^2 (SHELXL-97).⁸⁰ Non-hydrogen atoms were refined with anisotropic displacement parameters. Hydrogen atoms were placed in idealized positions and refined using a riding model with fixed isotropic contributions if possible. Reinvestigation of the crystal data of **3b** (in the BF_4 salt, previously published²⁰) yielded a so far unnoticed disorder (sof: 0.2) of the carbene ligand. Refinement of the less occupied site was supported by restraining its geometry to fit the major ligand site using SAME. All crystals were found to contain

(76) *SADABS* (version 2.05); Bruker AXS Inc.: Madison, WI, 2002.

(77) *SAINT: Data reduction software* (version 6.45); Bruker AXS Inc.: Madison, WI, 2003.

(78) *SMART: Data collection software* (version 5.629); Bruker AXS Inc.: Madison, WI, 2003.

(79) Blessing, R. H. *Acta Crystallogr. A* **1995**, *51*, 33.

(80) Sheldrick, G. M. *Acta Crystallogr. A* **2008**, *64*, 112.

Table 4. Crystal Data, Data Collection, and Structure Refinement Details

	3b		4b
empirical formula	C ₄₂ H ₃₇ ClNP ₂ Pd·CF ₃ O ₃ S		C ₄₂ H ₃₇ ClNNiP ₂ ·CF ₃ O ₃ S
<i>M_r</i>	908.59		860.90
cryst syst	monoclinic		monoclinic
space group	<i>P</i> 2(1)/ <i>n</i>		<i>P</i> 2(1)/ <i>n</i>
<i>a</i> /Å	14.672(5)		14.6778(18)
<i>b</i> /Å	18.609(6)		18.491(2)
<i>c</i> /Å	18.404(6)		18.317(2)
α/deg	90		90
β/deg	107.724(5)		109.068(2)
γ/deg	90		90
<i>V</i> /Å ³	4786(3)		4698.6(10)
ρ _{calc} /g cm ⁻³	1.261		1.217
<i>Z</i>	4		4
<i>F</i> (000)	1848		1776
μ(Mo Kα/mm ⁻¹)	0.60		0.63
<i>T</i> /K	100		100
refls measd	24 537		23 577
refls unique	8709 [<i>R</i> _{int} = 0.117]		8384 [<i>R</i> _{int} = 0.031]
refined params/restraints	497/1		497/0
<i>R</i> ₁ [<i>I</i> ≥ 2σ(<i>I</i>)]	0.068		0.042
<i>wR</i> ₂ ^a	0.181		0.113
weighting scheme ^a	<i>a</i> = 0.0896 <i>b</i> = 0.000		<i>a</i> = 0.0617 <i>b</i> = 0.1765
σ _{fin} (max./min.)/e Å ⁻³	1.34/−1.50		0.66/−0.33
	6·2CH ₂ Cl ₂	7·CH ₂ Cl ₂	9a
empirical formula	C ₄₂ H ₃₆ Cl ₂ NP ₂ Pd·CF ₃ O ₃ S·2(CH ₂ Cl ₂)	C ₄₂ H ₃₆ Cl ₂ NNiP ₂ ·CF ₃ O ₃ S·CH ₂ Cl ₂	C ₄₆ H ₃₈ Cl ₂ NP ₂ Pd·CF ₃ O ₃ S
<i>M_r</i>	1112.88	980.26	993.08
cryst syst	monoclinic	monoclinic	monoclinic
space group	<i>P</i> 2(1)/ <i>c</i>	<i>P</i> 2(1)/ <i>n</i>	<i>C</i> 2/ <i>c</i>
<i>a</i> /Å	17.6792(17)	10.5898(7)	25.183(6)
<i>b</i> /Å	16.9370(17)	21.8258(14)	11.472(2)
<i>c</i> /Å	16.3414(16)	19.7422(13)	34.952(7)
α/deg	90	90	90
β/deg	106.954(2)	104.7130(10)	99.278(4)
γ/deg	90	90	90
<i>V</i> /Å ³	4680.5(8)	4413.4(5)	9966(4)
ρ _{calc} /g cm ⁻³	1.579	1.475	1.324
<i>Z</i>	4	4	8
<i>F</i> (000)	2248	2008	4032
μ(Mo Kα) (mm ⁻¹)	0.91	0.86	0.63
<i>T</i> /K	100	100	100
refls measd	24 156	23 126	26 296
refls unique	731 [<i>R</i> _{int} = 0.034]	8048 [<i>R</i> _{int} = 0.028]	9103 [<i>R</i> _{int} = 0.047]
refined params /restraints	560/0	533/0	542/2
<i>R</i> ₁ [<i>I</i> ≥ 2σ(<i>I</i>)]	0.053	0.038	0.042
<i>wR</i> ₂ ^a	0.120	0.095	0.097
weighting scheme ^a	<i>a</i> = 0.0457 <i>b</i> = 17.9112	<i>a</i> = 0.048 <i>b</i> = 3.1369	<i>a</i> = 0.0534 <i>b</i> = 0.000
σ _{fin} (max./min.)/e Å ⁻³	1.67/−1.56	0.72/−0.59	0.91/−0.54

$$^a wR_2 = \{ \sum [w(F_o^2 - F_c^2)^2] / \sum [w(F_o^2)^2] \}^{1/2}; w = 1 / [\sigma^2(F_o^2) + (ap)^2 + bp]; p = (F_o^2 + 2F_c^2) / 3.$$

solvent. In **3b**, **4b**, and **9a** the dicholormethane molecules could not be resolved due to disorder and were thus removed by the SQUEEZE routine in PLATON.⁸¹ Detailed information about the solvent-accessible void and removed electrons can be found in the CIF along with a complete list of displacement parameters and tables of interatomic distances and angles. These have been deposited with the Cambridge Crystallographic Data Centre and can be obtained free of charge via www.ccdc.cam.ac.uk/data_request/cif on quoting CCDC 796954 to 796958 and 797119.

Computational Section

With the exception of **M6**, **M7**, **M6'**, and **M7'** (BP86/TZVPP), all geometries were optimized under *C_s*-symmetry constraint using density functional theory at the BP86 level of theory^{82,83}

using uncontracted Slater-type orbitals (STOs) with TZ2P quality as basis functions for the SCF calculations.⁸⁴ An auxiliary set of s, p, d, f, and g STOs was used to fit the molecular densities and to represent the Coulomb and exchange potentials accurately in each SCF cycle.⁸⁵ Scalar relativistic effects have been incorporated by applying the zeroth-order regular approximation (ZORA).⁸⁶ The nature of the stationary points on the potential energy surface was determined by calculating the vibrational frequencies. All structures are minima on the potential energy surface.

The bonding situation of the metal–carbene bonds was investigated by an energy decomposition analysis that was developed by Morokuma⁸⁷ and by Ziegler and Rauk.^{88,89} The

(84) Snijders, J. G.; Vernooijs, P.; Baerends, E. *At. Data Nucl. Data Tables* **1981**, 483.

(85) Krijn, J.; Baerends, E. J., *Fit Functions in the HFS-Method*; Internal Report (in Dutch); Vrije Universiteit Amsterdam, The Netherlands, 1984.

(86) vanLenthe, E.; vanLeeuwen, R.; Baerends, E. J.; Snijders, J. G. *Int. J. Quantum Chem.* **1996**, 57, 281.

(81) Spek, A. L. *J. Appl. Crystallogr.* **2003**, 36, 7.

(82) Becke, A. D. *Phys. Rev. A* **1988**, 38, 3098.

(83) Perdew, J. *Phys. Rev. B: Condens. Matter* **1986**, 34, 7406.

bonding analysis focuses on the instantaneous interaction energy ΔE_{int} of a bond A–B between two fragments A and B in the particular electronic reference state and in the frozen geometry of AB. This interaction energy is divided into three main components [eq 1].

$$\Delta E_{\text{int}} = \Delta E_{\text{elstat}} + \Delta E_{\text{Pauli}} + \Delta E_{\text{orb}} \quad (1)$$

The term ΔE_{elstat} corresponds to the classical electrostatic interaction between the unperturbed charge distributions of the prepared atoms and is usually attractive. The Pauli repulsion, ΔE_{Pauli} , is the energy change associated with the transformation from the superposition of the unperturbed electron densities $\rho_A + \rho_B$ of the isolated fragments to the wave function $\Psi^0 = N \hat{A} [\Psi_A \Psi_B]$, which properly obeys the Pauli principle through explicit antisymmetrization (\hat{A} operator) and renormalization of the product wave function.⁹⁰ It comprises the destabilizing interactions between electrons of the same spin on either fragment. The orbital interaction ΔE_{orb} accounts for charge transfer and polarization effects.⁹¹ The ΔE_{orb} term can be decomposed into contributions from each irreducible representation of the point group of the interacting system. This makes it possible to estimate the intrinsic strength of orbital interactions from orbitals having a' (σ) and a'' (π) symmetry quantitatively. To obtain the bond dissociation energy, D_e , the preparation energy, ΔE_{prep} , which gives the relaxation of the fragments into their

electronic and geometrical ground states, must be added to ΔE_{int} [eq 2].

$$\Delta E (= -D_e) = \Delta E_{\text{int}} + \Delta E_{\text{prep}} \quad (2)$$

To calculate the dissociation energies, we calculated each fragment in its optimized geometry and derived ΔE by eq 2. Further details on the EDA can be found in the literature.^{90,92} The EDA has been used by us for a comprehensive study of metal–ligand interactions in transition metal complexes.^{93,94}

Acknowledgment. We are very grateful to Dr. Ralf Tonner, whose additional calculations helped to settle questions that arose during the peer-review process. We also thank the South African National Research Foundation for financial support. E.S. thanks SASOL for a Ph.D. scholarship, O.S., S.C., and H.G.R. appreciate support from the Alexander von Humboldt Foundation, and OS thanks the German Academy of Sciences Leopoldina (BMBF LPD 9901/8-179). G.H. further thanks the DAAD (grant number A/05/52686) for postdoctoral funding. M.A. is very grateful for an Alfred Werner Assistant Professorship.

Supporting Information Available: Crystallographic details as CIF; ORTEP figure of **3a** (in the BF_4 salt) with resolved disorder; correlation of calculated charges and ^{13}C NMR data in chloropyridines; average geometries of chloropyridinium salts; Cartesian coordinates for all calculated structures. This material is available free of charge via the Internet at <http://pubs.acs.org>.

-
- (87) Morokuma, K. *J. Chem. Phys.* **1971**, *55*, 1236.
 (88) Ziegler, T.; Rauk, A. *Inorg. Chem.* **1979**, *18*, 1755.
 (89) Ziegler, T.; Rauk, A. *Inorg. Chem.* **1979**, *18*, 1558.
 (90) Bickelhaupt, F. M.; Baerends, E. J. In *Reviews in Computational Chemistry*, Vol. 15; Wiley-VCH: New York, 2000.
 (91) Bickelhaupt, F. M.; Nibbering, N. M. M.; van Wezenbeek, E. M.; Baerends, E. J. *Phys. Chem.* **1992**, *96*, 4864.
 (92) Velde, G. T.; Bickelhaupt, F. M.; Baerends, E.; Guerra, C. F.; Van Gisbergen, S. J. A.; Snijders, J. G.; Ziegler, T. *J. Comput. Chem.* **2001**, *22*, 931.

-
- (93) Frenking, G.; Wichmann, K.; Fröhlich, N.; Loschen, C.; Lein, M.; Frunzke, J.; Rayon, V. M. *Coord. Chem. Rev.* **2003**, *238*, 55.
 (94) Lein, M.; Frenking, G. In *Theory and Application of Computational Chemistry: The First Forty Years*; Dykstra, E., Frenking, G., Kim, K. S., Scuseria, G. E., Eds.; Elsevier: Amsterdam, 2005.